Cortical Microcircuitry of Executive Control and Source of Associated Event-Related Potentials

Amirsaman Sajad[1*], Steven P. Errington[1*], & Jeffrey D. Schall[1,2]

[1] Department of Psychology, Vanderbilt Vision Research Center, Center for Integrative & Cognitive Neuroscience, Vanderbilt University, Nashville, TN

[2] Centre for Vision Research, Vision Science to Application, Department of Biology, York University, Toronto, ON

[*] authors contributed equally to this work.

Corresponding author:

Jeffrey D. Schall, Ph.D.

E-mail: schalljd@yorku.ca

Medial frontal cortex enables executive control by signaling conflict, monitoring and predicting events and outcomes, and goal maintenance, indexed by event-related potentials (ERP). In monkeys performing a saccade countermanding (stop-signal) task, we recorded EEG over and neural spiking across all layers of the supplementary eye field (SEF). Neurons did not contribute to reactive response inhibition. Those signaling response conflict and tracking and predicting the timing of events for successful stopping had different spike widths and were concentrated differently across layers. Conflict neurons were in all layers and those encoding temporal parameters were concentrated in L2/3 and L5. The N2 indexed reward association with variation of polarization predicted by conflict and event timing neurons in L2/3 but not L5/6. The P3 indexed the timing of the upcoming event with variation of polarization predicted by event timing neurons in L2/3 but not L5/6. These findings reveal novel features of the cortical microcircuitry supporting executive control and producing associated ERP.

Effective control of behavior is necessary to achieve goals, especially when faced with competing instructions inducing response conflict and requiring inhibition of prepotent responses, maintenance of task goals, and adaptation of performance. These features of executive control are investigated with the countermanding (stop-signal) task [1], during which macaque monkeys, like humans, exert response inhibition and adapt performance based on stimulus history, response outcomes, and the temporal structure of task events [2].

Medial frontal cortex enables executive control, but circuit-level mechanisms remain uncertain [3, 4]. Hypotheses have been tested using the noninvasive measure of the N2 and P3 ERP in humans [5], but these have not been described in macaque monkeys. Mechanistic hypotheses about the basis of these signals require information about neural spiking patterns across cortical layers [6]. We can obtain such information from the supplementary eye field (SEF), an agranular area on the dorsomedial convexity in macaques, which contributes to proactive but not reactive response inhibition [7], contributes to working memory [8, 9], and signals surprise [10], event timing [11], response conflict, errors, and reinforcement [12]. SEF in macaques is homologous to SEF in humans [13]. SEF activation improves performance in the countermanding task by delaying response time [14] through postponing the accumulation of pre-saccadic activity [15].

The canonical cortical microcircuit derived from granular sensory areas [16] does not explain agranular frontal areas like SEF [17-20]. We recently described the laminar microcircuitry of error, reward gain, and reward loss neurons in SEF, finding that neural modulation in upper layers (layers 2 and 3; L2/3) but not lower layers (layers 5 and 6; L5/6) predicts the amplitude of the event-related potential and adaptation of response time associated with errors [12]. Here we

describe the laminar microcircuitry of other neurons that signal response conflict and monitor or predict event timing associated with inhibitory control. We also show that macaque monkeys produce the N2/P3 ERP associated with response inhibition and how SEF spiking predicts the ERP.

RESULTS

Countermanding performance, neural sampling, and functional classification.

Neurophysiological and electrophysiological data was recorded from two macaque monkeys performing the saccade countermanding task with explicit feedback tone cues (**Fig. 1a**) [21]. Data collection and analysis was informed by the consensus guide for the stop-signal task [22]. In 29 sessions we acquired 33,816 trials (Monkey Eu, male, 12 sessions 11,583 trials; X, female, 17 sessions 22,233 trials). Typical performance was produced by both monkeys. Response times (RT) on failed inhibition trials (noncanceled trials) (mean ± SD Eu: 294 ± 179 ms; X 230 ± 83 ms) were systematically shorter than those on no-stop trials (Eu: 313 ± 119 ms, X: 263 ± 112 ms; mixed effects linear regression grouped by monkey, $t(27507) = -17.4$, $p < 10^{-5}$) (**Fig. 1b**). Characteristically, the probability of noncanceled errors increased with stop-signal delay (SSD) (**Fig. 1b**). These two observations validate the use of the independent race model [23] to estimate the stop-signal reaction time (SSRT), the time needed to cancel a partially prepared saccade. SSRT across sessions (Eu: 118 ± 23 ms, X: 103 ± 24 ms) did not differ between monkeys ($t(27) = -1.69$, $p = 0.1025$). While there were other types of errors made in the task, they were infrequent and therefore inconsequential to this study. Therefore, by P (error) we refer to the probability of noncanceled errors.

EEG was recorded with leads placed on the cranial surface by the chamber over medial frontal cortex, and a linear electrode array (Plexon, 150 µm spacing) was inserted in SEF (**Fig. 1c**). SEF was localized by anatomical landmarks and intracortical electrical microstimulation [22]. We recorded neural spiking in 29 sessions (Eu: 12, X: 17) sampling activity from 5 neighboring sites. Overall, 575 single units (Eu: 244, X: 331) were isolated, of which 213 (Eu: 105, X: 108) were modulated after SSRT. The description of the laminar distribution of signals is based on 16 of the 29 sessions during which electrode arrays were oriented perpendicular to cortical layers and we could assign neurons to different layers confidently [18] (see Supplementary Fig. 1 of Sajad et al., 2019[12]). Additional information about laminar structure was assessed through the pattern of phase-amplitude coupling across SEF layers [20]. Due to variability in the estimates and the indistinct nature of the L6 border with white matter, some units appeared beyond the average gray-matter estimate; these were assigned to the nearest cellular layer. In all, 119

isolated neurons (Eu: 54; X: 65) contributed to the results on laminar distribution of executive control signals subserving successful stopping (**Supplementary Table 1a)**.

To identify neural activity associated with saccade countermanding, we examined the activity across different stop-signal delays on Canceled trials in which the subject successfully inhibited the movement, and latency-matched No-stop trials in which no stopping was required [24]. A consensus cluster algorithm [25] with manual curation identified neurons with response facilitation (n = 129) and response suppression (n = 84) following the stop-signal (**Supplementary Figure 1**). Simultaneously, we observed distinct patterns in the cranial EEG exhibited related to successful stopping with characteristic N2 and P3 components (**Fig 1c**).

To determine possible contributions of the diverse neurons, we compared and contrasted how well neural signals related to a variety of computational parameters inherent in the task. The primary time periods of interest were the interval preceding SSRT and the interval after SSRT before the feedback tone, which terminated operant control on behavior.

First, performance of the stop-signal task is explained as the outcome of a race between stochastic GO and STOP processes [23], instantiated by specific interactions enabling the interruption of the GO process by a STOP process [26, 27] (**Supplementary Figure 2a**). An influential theory of medial frontal function posits that it encodes the conflict between mutually incompatible processes [28]. Such conflict arises naturally as the mathematical product of the activation of GO and STOP units, which is proportional to P (error). Hence, neural signals that scale with P (error) can encode conflict in this task.

Second, inspired by reinforcement learning models, we considered the possibility that neural signals reflect the error-likelihood associated with an experienced SSD [29]. Note that in a proportion of stop-signal error trials, the response was generated prior to SSD. The error-likelihood can only form based on trials in which SSD elapsed before RT (referred to as SSD_{seen}). Hence, neural signals that scale with P (error | SSD_{seen}) can encode error-likelihood in this task. While correlated in this task, conflict (P (error)) and error likelihood (P (error | SSD_{seen})) diverge at longer SSDs (**Supplementary Figure 2c**).

Third, to earn reward in this task, monkeys learn the timing of the various task events (**Supplementary Figure 2b**). For example, monkeys are sensitive to the adjustments of SSD that are made to maintain ~50% success on stop-signal trials [30]. Previous research has described the characteristics of time perception [31-33]. Key characteristics include sensitivity to log(interval) versus its absolute value with precision decreasing with duration and sensitivity to the moment-by-moment expectation (i.e., hazard rate) of events (**Supplementary Figure 2d-e**). Therefore, neural activity around the time of SSD can scale with the timing or expectation of the

stop-signal [11, 34, 35]. This expectation must be derived only from experienced SSD and estimated probability that the stop-signal would occur on a given trial (**Supplementary Figure 2e**). Moreover, to earn reward, monkeys were required to maintain fixation on the target on trials with no stop-signal or on the fixation spot on canceled trials for an extended period until a tone secondary reinforcer (feedback) announced delivery of reward after another interval. Hence, neural signals that scale with the duration of SSD_{seen} or the delay until the feedback tone can encode time (**Supplementary Figure 2d**).

Mixed-effects model-comparison based on Bayesian Information Criteria (BIC) was used to resolve these alternatives (see **Methods**). As detailed below, 75 neurons signaled Conflict and 138 signaled aspects of the timing of events critical for executive control.

Monitoring Conflict. Previously, this laboratory reported neurons in SEF with transient facilitation after SSRT on canceled trials that was proportional to P (error) [36]. We replicated that observation, finding 75 such neurons **(Fig. 2; Supplementary Figure 3)**. This modulation was not a visual response to the stop-signal because it did not happen on noncanceled trials (**Supplementary Figure 1e**). A minority of these neurons produced weak, persistent activity on Canceled trials that lasted until the tone, and some also exhibited a brief transient response following the tone (**Fig. 2; Supplementary Figure 1c**).

We assessed how the magnitude of this transient modulation after SSRT varied with conflict and timing factors. Amongst the tested models, the magnitude of this modulation varied with P (error) (Mixed-effects linear regression grouped by neuron, $t(104) = 3.57$, $p = 0.00054$). This model was better (i.e., obtained the lowest BIC) compared to SSD or any other quantity, with weak support against the P (error | SSDseen) ($\Delta BIC = 1.29$) and strong support against other models ($\Delta BIC > 2.7$) (**Fig 2c; Supplementary Table 2a;** see **Methods** section *Model Comparison*). In contrast, the spike rate immediately before the feedback tone was unrelated to any factor related to its time or anticipation.

We noted that the vast majority (65/75) of these neurons did not signal noncanceled errors, supporting previous findings (**Supplementary Table 4**) [12, 36]. However, many (41/75) also exhibited modulation following the Feedback tone and around the time of reward. Some exhibited higher discharge rate on unrewarded than rewarded trials (previously identified as Loss signal [12]), and some exhibited higher discharge rate on rewarded trials than unrewarded trials (previously identified as Gain signal [12]). The relative multiplexing of Conflict neurons with Gain and Loss signals did not significantly differ from chance level (X^2 (3, N = 575) = 1.02, p = 0.79).

The neurons encoding conflict were found at all recording sites but more commonly at some (X^2 (4, N = 575) = 11.6, p = 0.020). Using trough-to-peak duration of the action potential waveform, we inferred whether neurons were putative pyramidal neurons with broad spikes or interneurons with narrow spikes. The majority (63/75) had broad spikes. This distribution did not differ from the overall sampling distribution in SEF (X^2 (1, N = 575) = 0.67, p = 0.41).

On average, the conflict signal in these neurons started 99 ± 8 ms (mean ± SEM) after SSRT with nearly all (71/75) recruited only after SSRT. The proportion of recruited neurons reached a maximum of ~60% at ~110 ms after SSRT and gradually reduced to 8% after 500 ms (**Fig. 2a**). Because this facilitation occurs after SSRT, it cannot contribute to reactive response inhibition.

From sessions with perpendicular penetrations, we assigned 36 of the 75 neurons to a cortical layer. They were found in all layers at a relative prevalence across layers similar to that of the overall sampling distribution (X^2 (4, N = 293) = 4.28, p = 0.37; **Fig 2b; Supplementary Table 1b**). The timing of the modulation did not differ between L2/3 and L5/6 (*t*-test, t (34) = 0.3367, p = 0.74). The few neurons with peri-tone modulation were observed sparsely across all layers.

In summary, as reported previously [36], neurons in SEF modulate in a manner consistent with signaling the co-activation of gaze-shifting (GO) and gaze-holding (STOP) processes. This co-activation has previously been interpreted as conflict [28, 37] The new results show that these neurons are distributed across all SEF layers and predominantly are putative pyramidal neurons with broad spikes.

Time keeping. Besides resolving the conflict between going and stopping, this task requires maintenance of response inhibition for an arbitrary interval. To earn reward on canceled trials, monkeys were required to maintain gaze fixation on the stop-signal until an auditory feedback tone occurred. Monkeys adapt performance by learning the temporal regularities of the task [30, 38]. Extending previous research describing neural signals in SEF signaling interval timing [11], and supporting working memory [9], we identified neurons across the layers of SEF with modulation through task intervals that can represent the timing of task events through facilitation, suppression, and ramping activity [35, 39]. We will describe two populations of neurons that signal the timing of task events related to stopping performance, the timing of the feedback tone, and the duration of control (**Supplementary Fig 2c, d**).

Following target presentation, the discharge rate of many neurons (N = 84) increased and persisted until the saccade on trials with no stop-signal or noncanceled error trials. On

canceled trials, the discharge rate was abruptly reduced after SSRT (**Fig 3a; Supplementary Fig 1c-e**). A subset of these neurons (~35%) exhibited monotonic ramping of discharge rate following the sharp suppression, persisting until after the feedback tone whereupon the spike rate again decreased. In some neurons this decrease followed a brief transient response (**Fig 3a**).

The first pronounced suppression began after SSRT, so these neurons cannot contribute directly to response inhibition. Relative to SSRT, the time at which these neurons suppressed preceded the facilitation in the conflict monitoring neurons (t-test, t (157) = -3.60, p = 4.2×10^{-4}). Variations in the ramping activity before SSRT was best described by the time-based models of SSD (Mixed-effects Linear Regression grouped by neuron, t (250) = 12.62, p = 0.0013) with strong support against other models (Δ BIC > 2.7) (**Supplementary Table 2**). The log-transformed model outperformed the linear model but evidence against the linear model was weak (ΔBIC = 1.35). Because the discharge rate dropped sharply on successful canceled trials but not on noncanceled stop-signal trials (**Supplementary Fig 1e**), we conjecture that these neurons encode the temporal aspects of events leading to successful stopping and not the timing of the stop-signal appearance per se. Once successful stopping occurs these neurons are suppressed.

The variation in dynamics of the ramping before the tone was best accounted for by the time of the feedback tone from the appearance of the stop-signal (Mixed-effects Linear Regression grouped by neuron, t (112) = 3.41, p = 0.00091) with strong support against other models (Δ BIC > 5.0). The linear and log-transformed models were indistinguishable (ΔBIC < 0.1) (**Supplementary Table 2**). The termination of this modulation was best described by the time of the feedback tone and not the time at which fixation from stop-signal was broken (**supplementary Figure 4c)** confirming that this ramping activity occurs in anticipation of the tone but is not associated with direct control of the behavior.

Based on the ramping observed before the stop-signal and tone events, best explained by the time-based models, and the suppression following both events, we conjecture that these neurons represent time-keeping signals important to accomplish the task. Therefore, henceforth we refer to these neurons as ‘Event Timing’ neurons.

Event Timing neurons were found in all penetrations, but more commonly in certain sites (X^2 (4, N = 575) > 39.3, p < 10^{-5}) (**Supplementary Table 1a**). The majority (73 / 84) had broad spikes. This distribution did not differ from the overall sampling distribution in SEF (X^2 (1, *N = 575*) = 2.56, p = 0.11). From sessions with perpendicular penetrations, we assigned the layer of 49 of the 84 neurons. These neurons appeared more common in L3 and L5, but their incidence

did not differ from the overall laminar sampling distribution (X^2 (4, N = 293) = 7.33, p = 0.12). However, those with ramping activity before the tone were more confined to lower L3 and upper L5 (**Fig 3c**). The time of modulation after SSRT or around the tone did not vary across layers.

Feedback Time Prediction and Goal Maintenance. Many other neurons (N = 54) in SEF produced modestly elevated discharge rates persisting until after the tone on trials with no stop-signal, but most characteristically on canceled trials they produced significantly greater discharge rates after presentation of the stop-signal. The modulation was not just a response to the stop-signal because it did not happen on noncancelled error trials (**Supplementary Figure 1d, e**).

These neurons were distinguished from conflict monitoring neurons based on the duration of this facilitation coupled with the spike rate modulation synchronized on the feedback tone (**Supplementary Figure 1b, c**). The time of peak recruitment of these neurons (~300 ms) followed that of the neurons monitoring conflict (~110 ms) and the suppression of the neurons representing event time (~170 ms). The phasic facilitation of a significantly higher proportion of these neurons compared to conflict monitoring neurons was followed by prolonged elevated discharge rate lasting until a brief period (~300 ms) following the auditory feedback tone (X^2 (1, N = 129) = 27.3, $p < 10^{-5}$) (**Fig 4a**). This modulation at tone presentation was also observed on no-stop trials.

The modulation on canceled relative to no-stop trials started after SSRT, too late to contribute to reactive response inhibition. The variation in magnitude of the phasic modulation was best accounted for by the log-transformed time of the feedback tone on canceled trials (**Fig 3d**) (Mixed-effects Linear Regression grouped by neuron, t (152) = 3.53, p = 0.00056, with strong evidence against non-time-based models (Δ BIC > 3.0) and weak evidence against other time-based models (ΔBIC < 1) (**Supplementary Table 3**).

We did additional analyses to determine whether the sustained activity that followed the phasic response is directly tied to the control of behavior, the cue indicating release of control (i.e., feedback tone irrespective of its valence), or the occurrence of the secondary reinforcement (i.e., positive feedback tone). First, the termination of this modulation was not related to the time at which fixation on the stop-signal was broken, ruling out this signal as one directly involved in maintaining fixation on the stop-signal (**Supplementary Figure 5c**). Furthermore, when the feedback tone cued upcoming reward, the activity dropped but when it cued failure, it increased (**Supplementary Figure 5d**). This explains why a significant proportion of these neurons multiplexed Loss signal following the tone, with a higher prevalence

than chance (X^2 (3, N = 575) = 19.43, p = 0.00022). These results show that the temporal dynamics of neural response around the time of the feedback tone is linked to its time and valence.

In summary, these neurons generate sustained activity until the secondary reinforcement. The pattern of this modulation encodes the duration of the interval based on the temporal association acquired through training. Furthermore, the sustained activity following the phasic response can maintain this representation until the feedback is provided, when operant control on behavior is released. Based on the temporally extended nature of the task design and previous findings identifying SEF signals with working memory [8, 9], we conjecture that these neurons sustain the representation of canceling the saccade necessary to earn reward. Hence, we refer to these neurons as 'Goal Maintenance' neurons.

Goal Maintenance neurons were found in all penetrations but were more common at certain sites (X^2 (4, N = 575) > 39.3, p < 10^{-5}). One third (18/54) were narrow-spiking, a proportion significantly greater than expected by chance (X^2 (1, N = 575) = 7.29, p = 0.0069). The laminar distribution of Goal Maintenance neurons (**Fig. 4c**) was significantly different from the laminar sampling distribution (X^2 (4, N = 293) = 11.24, p = 0.024) (**Supplementary Table 1b**). These neurons were found significantly more often in L2/3 relative to L5/6 (X^2 (1, N = 293) = 10.37, p = 0.00013. Their laminar distribution was also significantly different from that of Conflict neurons (X^2 (1, N = 70) = 11.54, p = 0.00068) and Event Timing neurons (X^2 (1, N = 83) = 5.49, p = 0.019). Furthermore, those in L2/3 modulated significantly earlier than those in L5/6 (L2/3 ~85 ± 64 ms (mean ± SD), L5/6 ~ 193 ± 101; *t*-test, t (32) = -3.63, p = 0.00099).

Overall, the results of Event Timing and Goal Maintenance neurons described above indicates that sustained facilitation, suppression, and ramping of spike rates in SEF can encode the time of critical task events. The differences in temporal dynamics of these neurons and their laminar distribution suggests that they can contribute to distinct processes.

Countermanding N2 ERP. To determine whether macaque monkeys produce ERP components associated with response inhibition homologous to humans [5], we simultaneously sampled EEG from an electrode located over the medial frontal cortex (Fz in 10-20 system) while recording neural spikes in SEF (**Fig. 5a**). To eliminate components associated with visual responses and motor preparation and to isolate signals associated with response inhibition, we measured the difference in polarization on canceled trials and latency-matched no-stop trials for each SSD (**Fig. 5b**). Like humans, an enhanced N2/P3 sequence is associated with successful stopping.

The N2 began ~150 ms and peaked 222 ± 17 ms after the stop-signal, well after the visual ERP polarization (**Supplementary Fig 6a**). The N2 was observed after SSRT, too late to be a direct index of reactive response inhibition. Furthermore, the variability in the N2 peak time across sessions was significantly less when aligned on stop-signal appearance than on SSRT, providing further evidence dissociating the N2 from the act of stopping, ($F(28,28) = 0.29$, $p = 0.0018$, *F-test for variances*) (**Supplementary Fig 6c**). The variation in N2 amplitude was best accounted for by P (error | SSD_{seen}) (Δ BIC > 3.0 against competing models), with the largest negativity when the experienced SSD was the earliest and associated with the lowest error likelihood (Mixed-effects Linear Regression grouped by session, $t(85) = 2.42$, $p = 0.0178$) (**Fig 5c, Supplementary Table 2**). The failure of the other models adds to the conflicting and inconclusive results about N2 indexing conflict monitoring and response inhibition [5, 21].

We now describe relationships between neural spiking and the N2. **Figure 5b** illustrates the alignment between the N2/P3 ERP and the temporal recruitment of the three kinds of neurons described above. The N2 was more closely aligned with the peak recruitment of Conflict and of Event Timing neurons. The relationship between neural events in SEF and the voltages measured on the cranium above SEF is both biophysical and statistical. The cranial voltage produced by synaptic currents associated with a given spike must follow Maxwell's equations as applied to the brain and head no matter the temporal overlap between different events. Hence, we counted the spikes of the three classes of neurons described above separately, during a 100 ms window centered on the peak of the ERP separately in L2/3 and in L5/6. We devised multiple linear regression models with activity in upper layers (L2/3) and lower layers (L5/6) of each neuron type as predictors. Only successful canceled trials were included in this analysis. We found that the polarization of the N2 is significantly predicted by the spiking activity in L2/3 but not in L5/6 of Conflict neurons (Multiple Linear Regression; L2/3: $t(117) = -3.6$, $p = 0.00047$; L5/6: $t(117) = 0.046$, $p = 0.96$) and Event Timing neurons (L2/3: $t(97) = -4.60$, $p = 0.000013$; L5/6: $t(97) = 1.67$, $p = 0.097$) (**Fig 5d**). Specifically, when the discharge rate of these L2/3 neurons was higher, the N2 exhibited a stronger negativity. Interestingly, the N2 amplitude was also predicted by the spiking activity in L2/3 but not in L5/6 of other neurons that were not modulated for successful stopping around the time of SSRT and thus not described in this manuscript (L2/3: $t(317) = -2.51$, $p = 0.012$; L5/6: $t(317) = -1.60$, $p = 0.11$) but was not predicted by the phasic spiking of Goal Maintenance neurons (L2/3: $t(57) = -1.28$, $p = 0.21$; L5/6: $t(57) = 0.60$, $p = 0.52$) (**Supplementary Figure 7a**). Similar results were obtained when controlling for the variation of ERP polarization and spike rate across different SSDs (not

shown) and when we measured spiking activity and ERP by considering the differential activity (both ERP and spikes), subtracting out activity on No-stop trials (**Supplementary Figure 7b**).

Countermanding P3 ERP. The N2 was followed by a robust P3 (**Fig 5a, b**) beginning ~300 ms and peaking 358 ± 17 ms after the stop-signal, similar to the human P3. P3 peak time was better synchronized on the stop-signal than on SSRT ($F(28,28) = 0.44$, $p = 0.0345$, *F-test for variances*) (**Supplementary Fig 6c**). The variation in P3 amplitude was best accounted for by the log-transformed time of the feedback tone on canceled trials (Δ BIC > 4.0 against competing models) with weak support against other time-based models (Δ BIC < 1.30) (**Fig 5e, Supplementary Table 2**). The amplitude of P3 was largest for longer feedback time (Mixed-effects Linear Regression grouped by session, $t(85) = 3.72$, $p = 0.000352$). The conclusions of these results do not differ if the analyses are performed on the raw EEG polarization in these intervals.

Unlike the N2, the P3 peak occurred closer in time to peak recruitment Goal Maintenance neurons (**Fig 5b**). When the P3 arose, the recruitment of both Conflict and Event Timing neurons was decreasing. We found that the P3, unlike the N2, is significantly predicted by the spiking activity in L2/3 of Goal Maintenance neurons (Multiple Linear Regression; L2/3: $t(57) = 5.46$, $p = 0.0000011$; L5/6: $t(57) = 1.47$, $p = 0.15$) (**Fig. 5f**). When the discharge rate of these neurons is higher, the P3 exhibits a stronger positivity. P3 amplitude was not predicted by the spiking activity of Conflict neurons (L2/3: $t(97) = 0.44$, $p = 0.66$; L5/6: $t(97) = -0.49$, $p = 0.62$), Event Timing neurons (L2/3: $t(117) = -1.19$, $p = 0.24$; L5/6: $t(117) = -0.78$, $p = 0.44$), or neurons that were not modulated for successful stopping around the time of SSRT (L2/3: $t(317) = -1.11$, $p = 0.27$; L5/6: $t(317) = 0.054$, $p = 0.96$) (**Supplementary Figure 7c**). Once again, similar results were obtained when SSD was not controlled for (not shown) and when we measured spiking activity and ERP by considering the differential activity (both ERP and spikes), subtracting out activity on No-stop trials (**Supplementary Figure 7d**).

DISCUSSION

These new results offer fresh insights into the cortical microcircuitry supporting executive control in primates. They extend our previous description of the laminar structure of error and reward processing in SEF [12] and replicate patterns of neural spiking that have been described before but lacked laminar information during saccade countermanding and other tasks. We will discuss the possible contributions of SEF to conflict resolution and time estimation inherent in this task. The laminar organization of these diverse signals considered with knowledge of the connectivity

of SEF offers particular and unique constraints on neuro-computational models of executive control. Also, complementing our earlier description of the source of the ERN [12], we report a macaque homolog of the ERP components (N2/P3) associated with response inhibition. We will discuss additional insights into the cortical source of these ERP components.

Conflict processing and relationship with processing error and reward

The present results complement our previous description of the laminar organization of error and reward processing [36]. Neurons signaling noncanceled errors, reward gain or loss, and delivery of fluid reward had specific profiles of activity across cortical layers. Neurons signaling error or loss of reward were more common in L2/3, while neurons signaling gain of reward were more common in L5/6. We now describe other functional types of neurons in SEF.

One category was characterized by a pronounced facilitation after the stop-signal when saccades were inhibited. The modulation followed SSRT and the spike rate scaled with P (error). These neurons were predominantly broad spiking and found in all layers. We hypothesize that these neurons signal response conflict [36] as defined by Botvinick and colleagues [28]. In frontal eye field (FEF) and superior colliculus (SC) the gaze-shifting and gaze-holding neurons are co-active in a dynamically unstable manner that varies with P (error) precisely because these are the neurons producing the performance. In the interactive race model [26], the multiplicative conflict between GO and STOP accumulator units scales with P (error) and can be used to adjust interactive race parameters to accomplish post-stopping slowing [37]. Thus, this category of neuron signals a quantity central to theories of executive control. However, this signal is often distinct from error and reward because they are mostly found in different SEF neurons.

Further evidence dissociating conflict, reward, and error signals is offered by a recent investigation of the nigrostriatal dopamine system of monkeys performing saccade countermanding [40]. Dopamine (DA) neurons concentrated in the dorsolateral substantia nigra exhibited a pattern of activity that paralleled the conflict neurons in SEF. The DA neurons produced a brisk response to the stop-signal that was stronger when saccades were canceled in either direction. This observation is consistent with reports that besides responding to rewarding events, dopamine neurons respond to salient signals, such as a stop-signal. Unlike movement neurons in FEF [24] and SC [41] but like SEF, nearly all DA neurons modulate after SSRT. Moreover, the modulation of DA neurons scaled with P (error) just like the SEF neurons. SEF is innervated by DA neurons in Substantia Nigra pas compacta (SNpc) [42]. Axon terminals from SEF are rare in SNpc [43, 44] but dense in striatum [45]. Given the very slow conduction of DA

axons[46] and the well-known second-messenger delay of influence, we infer that the SEF modulation cannot be caused by DA inputs (**Supplementary Figure 8**). Instead, the DA responses can be derived from inputs from the SC, which is innervated by SEF and FEF.

Goal maintenance and time processing

Previously, the role of SEF and nearby areas in action timing and explicit time production tasks have been demonstrated [11, 34]. Here we show evidence for timing signals in the stop-signal task, a task with no explicit requirement for tracking intervals [47]. Nevertheless, because of the importance of the timing parameters (of SSD and duration of operant control), in this task monkeys can acquire the temporal statistics of events for optimal control [30]. We show evidence for SEF neurons with interval predicting phasic response followed by sustained facilitation that can serve goal maintenance (hence named Goal Maintenance neurons), and ramping neurons that can reflect time-keeping of specific events (hence named Event Timing neurons) [35, 39]. Specifically, the Event Timing neurons showed ramping activity before the stop-signal, followed by rapid response suppression in response to successful stopping, and slowly ramping activity before the feedback tone. Previously, the second phase of ramping was not described, and these neurons were identified as saccade-related in a loose sense because they cannot contribute to reactive inhibition. Now, we recognize another interpretation that incorporates more information.

Neurons in striatum of monkeys performing saccade countermanding exhibited parallel patterns of facilitation or suppression after the stop-signal that was stronger when saccades were canceled [40]. Similar to our results, the response facilitation and suppression occurred after SSRT. Once again, the parallels between SEF and the striatum in patterns of modulation associated with proactive but not reactive inhibition are unexpectedly clear. However, in that study, the temporal sequence of events following stopping was different from ours, so it remains unclear whether those neurons would exhibit similar time-predicting and time-tracking codes.

Extrinsic and Intrinsic microcircuitry of executive control

Coupled with extensive knowledge about extrinsic inputs and outputs of SEF [43-45], this new information about the laminar distribution of neurons signaling response conflict, event timing, and maintaining goals suggest several specific hypotheses and research questions about how SEF and associated structures accomplish response inhibition and executive control (**Fig. 7**).

Neurons signaling conflict were found in all layers. SEF can be informed about the dynamic state of gaze-shifting and gaze-holding through inputs from FEF and the thalamus.

Based on previous conjectures [6] and recent biophysical modelling [48] we hypothesize that the product of GO*STOP activation is derived through synaptic integration in L2/3. If this is so, and if the apical dendrites of L6 pyramidal neurons in SEF do not extend into L2/3, then this conflict signal can arise in L6 through translaminar interactions. The observation that conflict arises later in L6 is consistent with this supposition. Another implication of the hypothesis that conflict in L6 is derived from that in L2/3 is that the L6 feedback to thalamus will be delayed relative to the gaze-holding and gaze-shifting signals conveyed from the SC.

Goal Maintenance neurons were mainly found in L2/3. These neurons exhibited a phasic response that predicted the interval until the feedback tone and sustained discharge until the tone. Inputs to these neurons from dorsolateral prefrontal cortex (DLPFC) and anterior cingulate cortex (ACC) can signal the learned association between the current state and expected time of secondary reinforcer, the time during which operant control is enforced. Another source for this signal can be Ventral Tegmental Area (VTA) where similar time-predicting signals are observed[49]. The sustained discharge can be maintained through recurrent activation within SEF and between other structures [9, 50].

We propose that the Goal Maintenance neurons enforce the suppression of movements until the feedback tone announced that such suppression was no longer necessary. This can be accomplished if the pyramidal Goal Maintenance neurons project to the D2 neurons in the striatum [51]. Many Goal Maintenance neurons were also putative parvalbumin (PV) inhibitory neurons. Note, we inferred that the narrow spiking neurons described in this study are most commonly PV neurons because Calretinin (CR) and Calbindin (CB) neurons have relatively small somas concentrated in L2 and upper L3, whereas PV neurons have larger somas distributed more uniformly across all layers, similar to our narrow-spiking-neuron sampling distribution [12]. PV Goal Maintenance neurons can inhibit the D1 direct (action-promoting) pathway and the frontal eye field to suppress movement. As PV neurons in primates do not make direct extrinsic connections to distant brain areas, we propose that this is mediated by the inhibition of excitatory inputs to these motor structures (gray neurons). The push-pull mechanism of D1 and D2 pathways mediated by inhibitory and excitatory neurons is consistent with the observation that a significant proportion of these neurons also exhibit higher activity on unrewarded trials and influence post-error adjustments in RT in the next trial. Previously we proposed that the mechanism for this can be through similar influences on the D1 and D2 pathway [12]. Furthermore, the PV inhibitory neurons can be part of the intrinsic circuitry that mediates the balance in excitation and inhibition necessary for the maintenance of persistent activity in recurrent networks [52, 53]. Upon the occurrence of the anticipated event (i.e., feedback),

input from DLPFC and other interconnected frontal areas can drive the termination of this sustained activity by direct projections to CR and CB inhibitory neurons that can in turn suppress pyramidal and PV Goal Maintenance neurons, respectively [54]. Through this circuitry, Goal Maintenance neurons can contribute to executive control through sustained activity for predictable intervals.

Event Timing neurons exhibited ramping activity beginning after the visual target presentation and peaking at SSRT. Some of these neurons, particularly in L3 and L5 exhibited a second period of ramping activity preceding the tone. We conjecture that the appearance of the visual target initiates the first ramping activity, timing the interval until SSRT. This can provide a substrate for fronto-striatal pathways to learn, update, or validate the temporal structure of the task [55-57].

The ramping activity shuts off when successful stopping occurs. Successful stopping can be signaled by the resolution of the GO*STOP conflict achieved in the motor circuit, conveyed to SEF through afferents from FEF and oculomotor thalamus. Such inputs may be supplemented by other information from the thalamus [58], and stopping task rule from DLPFC and ventrolateral prefrontal cortex (VLPFC) [59]. A proportion of Conflict neurons were putative PV neurons that can suppress the Event Timing neurons. Alternatively, CR and CB neurons, mainly found in L2/3, can not only suppress L2/3 neurons, but they can also effectively suppress L5 neurons through specialized connections to their distal dendrites [60]. This suppression resets Event Timing neurons to ramp up again to the next duration i.e., the feedback tone. Tracking this time interval and learning its underlying structure is the mechanism through which the system can generate time predictions, manifested in the phasic response of our Goal Maintenance Neurons [55]. Therefore, the output from these neurons can be sent, via cortico-cortical connections, to areas like FEF involved in generation of movement, other areas in the limbic and cognitive cortex (including ACC and DLPFC), and the caudate nucleus.

The suppression in activity following SSRT and feedback tone can be mediated by the same circuit motif that drives the suppression of Goal Maintenance neurons following the feedback tone. Inputs that indicate successful stopping or the auditory feedback tone can directly activate inhibitory neurons. Because we did not observe such inhibitory neurons, it is possible that these are small CR inhibitory neurons that receive direct input from DLPFC and selectively inhibit pyramidal neurons [54]. SEF is an agranular structure with little or no interlaminar inhibitory connections [19], however CR neurons in the upper layers can still result in potent inhibition of L5 neurons through projections onto their distal dendrites [60].

Origin of Countermanding N2/P3

Here, we show that macaque monkeys exhibit a homologous N2/P3 complex and report that SEF is a source contributing to it [5]. We further illustrated that both the N2 and P3 were related to neural spiking of neurons in L2/3 and not L5/6, but this relationship was specific to some neuron types. These results offer useful new insights into the processes indexed by these ERP components.

Previously, we showed how the SEF contributes to the error-related negativity (ERN) [12]. We found that variations in error-related spiking in L2/3 but not in L5/6 predicted variation of EEG polarization across both error and correct trials. Because action potentials are not large or sustained enough to produce event-related potentials, we surmise that this neural spiking coincides with coherent current flow strong enough to produce in the ERN [48]. Similarly, our results suggest that the N2 and P3 can be generated by synaptic activity that occurs in L2/3.

There is no consensus on what the N2 indexes [61]. We report that the monkey N2 was similar in general features to the human N2 during the stop-signal task. However, we found that the amplitude of the N2 was best described by the likelihood of error associated with experienced stop-signal delays, and not conflict and stop-signal delay as previously suggested [5, 62]. Further, we demonstrate that the spiking of different types of neurons in L2/3 (but not L5/6) predicted the magnitude of the N2 component. Specifically, the N2 was associated with higher activity of Conflict neurons and Event Timing neurons, but also other neurons that did not modulate around the time of successful stopping. Therefore, it is possible that the N2 is under the influence of different processes that co-occur in distinct neuronal populations. This can explain the disagreement in the literature about the nature of this ERP component. The observation that N2 amplitude was not predicted by Goal Maintenance neurons can refine hypotheses about the origin of this ERP component.

The post stop-signal P3 component in our task exhibited similar features to that reported in humans [5]. Our results show that the amplitude of P3 was best described by the temporal parameters of the task, specifically the time of the expected feedback. This is in agreement with previous reports of P3 involvement in expectation, and temporal aspects of behavior [61].

In agreement with this interpretation, we found that the spike rate of Goal Maintenance neurons (in L2/3), which exhibit a time-predicting phasic response at the time of P3, but not that of Conflict and Event Timing neurons, predicted the amplitude of P3 on a trial-by-trial basis. Therefore, the P3, at least in our experimental design can index processes linked to temporal prediction and monitoring subserving Goal Maintenance.

Conclusion

These results validate the tractability of formulating neural mechanism models of performance monitoring and executive control, especially when constrained by formal, algorithmic [26], and spiking network [63] models of performance of a task with clear clinical relevance [64]. Pioneering insights into the microcircuitry and mechanisms of primary visual cortex began by describing the properties of neurons in different layers [65]. The present results complete the first catalogue for the SEF. Being an agranular area, contrasts with primary sensory areas will reveal the degree of computational uniformity across cortical areas. Being a source contributing to ERPs indexing performance monitoring and executive control, details about laminar processing in SEF will offer unprecedented insights into the microcircuitry of executive control.

METHODS

Animal care and surgical procedures. Data was collected from one male bonnet macaque (Eu, *Macaca Radiata*, 8.8kg) and one female rhesus macaque (X, *Macaca Mulatta*, 6.0kg) performing a countermanding task [18, 21]. All procedures were approved by the Vanderbilt Institutional Animal Care and Use Committee in accordance with the United States Department of Agriculture and Public Health Service Policy on Humane Care and Use of Laboratory Animals.

Surgical details have been described previously [66]. Briefly, magnetic resonance images (MRIs) were acquired with a Philips Intera Achieva 3T scanner using SENSE Flex-S surface coils placed above or below the animal's head. T1-weighted gradient-echo structural images were obtained with a 3D turbo field echo anatomical sequence (TR = 8.729ms; 130 slices, 0.70mm thickness). These images were used to ensure Cilux recording chambers were placed in the correct area (Crist Instruments). Chambers were implanted normal to the cortex (Monkey Eu: 17°; Monkey X: 9°; relative to stereotaxic vertical) centered on midline, 30mm (Monkey Eu) and 28mm (Monkey X) anterior to the interaural line.

Data collection protocol. An identical daily recording protocol across monkeys and sessions was carried out. In each session, the monkey sat in an enclosed primate chair with their head restrained 45cm from a CRT monitor (Dell P1130, background luminance of 0.10 cd/m2). The monitor had a refresh rate of 70Hz, and the screen subtended 46 ° x 36 ° of the visual angle. After advancing the electrode array to the desired depth, they were left for 3 to 4 hours until recordings stabilized across contacts. This led to consistently stable recordings with single units typically held indefinitely. Once these recordings stabilized, an hour of resting-state activity in near-total darkness was recorded. This was followed by the passive presentation of visual flashes followed by periods of total darkness in alternating blocks. Finally, the monkey then performed approximately 2000 to 3000 trials of the saccade countermanding (stop-signal) task, reported below.

Countermanding task. The countermanding (stop-signal) task utilized in this study has been widely used previously [22]. Briefly, trials were initiated when monkeys fixated at a central point. Following a variable time period, drawn from an aging function to avoid anticipation for visual stimulus [38], the center of the fixation point was removed leaving an outline. At this point, a peripheral target was presented simultaneously on either the left or right hand of the screen, serving as saccade target.

Monkeys faced an asymmetric association between stimulus direction and reward. The lower reward was 0-50% of the higher reward amount, adjusted to encourage response to the low-reward stimulus. The stimulus-response mapping of location-to-high reward changed across blocks of trials, with block length on most sessions set at 10 to 30 correct trials [67].

On most trials the monkey was required to make an eye movement to the target (no-stop trials). However, on a proportion of trials the center of the fixation point was re-illuminated (stop-signal trials); this stop-signal appeared at a variable time after the target had appeared (stop-signal delay; SSDs). An initial set of SSDs, separated by 40-60 ms for Monkey Eu and 100ms for monkey X, were selected for each recording session. The delay was then manipulated through an adaptive staircasing procedure in which stopping difficulty was based on performance. When a subject failed to inhibit a response, the SSD was increased by up to 3 steps (randomly drawn) to increase the likelihood of success on the next stop trial. Similarly, when subjects were successful in their inhibition, the SSD was decreased by a random step to decrease the likelihood of success on the next stop trial. This procedure was employed to ensure that subjects failed to inhibit action on approximately 50% of all stop-signal trials.

On no-stop trials, the monkey was rewarded for making a saccade to the target. On stop-signal trials, the monkey was rewarded for withholding the saccade and maintaining fixation on the fixation spot. Following a correct response, an auditory tone was sounded 600ms later, and followed by a high or low fluid reward, depending on the stimulus-outcome mapping.

Performance on this task is measured by the probability of not canceling a saccade as a function of the SSD (inhibition function) and the distribution of latencies of correct saccades in no-stop-signal trials and of noncanceled error saccades in stop-trials (**Fig 1b; Supplementary Fig 2a**).

As performance on the stop-signal task can be considered as the outcome of a race between a GO and STOP process, then a stop-signal reaction time (SSRT) can be calculated [23]. This value can be considered as the latency of the inhibitory process that interrupts movement preparation [26, 63, 68]. SSRT was calculated using the weighted-integration method. Using this method, no-stop-trial RTs were rank-ordered and the RT value at the percentile which corresponded to the corresponding percentage of noncanceled stop trials for each SSD was calculated. The calculated SSRT was the average (weighted by number of trials) of the estimate obtained for each SSD. These SSRT values are contrasted against those calculated using a Bayesian parametric approach [69, 70] **(Supplementary Fig. 3a, 4a, 5a).** Compared to classical methods of calculating SSRT (i.e. integration-weighted method, Logan and Cowan [23]), this approach allows for a distribution of SSRT to be derived by using the distribution of reaction

times on no-stop trials, and by considering reaction times on noncanceled trials as a censored no-stop response time (RT) distribution. Furthermore, this model also allows for the estimation of the probability of trigger failures for a given session [71]. Individual parameters were estimated for each session. The priors were bounded uniform distributions (μ_{Go}, μ_{Stop}: U (0.001, 1000); σ_{Go}, σ_{Stop}: U (1, 500) τ_{Go}, τ_{Stop}: U (1, 500); pTF: U (0,1)). The posterior distributions were estimated using Metropolis-within-Gibbs sampling and we ran multiple (3) chains. We ran the model for 5000 samples with a thinning of 5. The conclusions of this study did not depend on the choice of SSRT calculation method.

Processing of neuronal activity

Analysis of spiking activity. Spike density functions (SDF) for individual trials were constructed by convolving the spike array with a kernel resembling a post-synaptic potential with an area equal to 1.

$$R(t) = \left\{1 - e^{\left(-\frac{t}{\tau_g}\right)}\right\} \cdot e^{\left(-\frac{t}{\tau_d}\right)}$$

In this kernel, the rate as a function of time, R(t), varies according to τ_g (the time constant for the growth phase, 1ms) and τ_d (the time constant for the decay phase, 20ms). This is similar to those observed in physiological data from excitatory synapses.

To study neural activity associated with successful stopping, we compared the activity on Canceled and latency-matched No-stop trials. This comparison revealed two distinctive patterns of modulation after successful stopping (i.e., SSRT). One group of neurons (N = 129) showed response facilitation and another group (N = 84) response suppression. This classification emerged from applying a clustering algorithm on SDFs at pre-determined time intervals (Lowe and Schall, 2018; See Methods) (Supplementary Fig 1B). Specifically, the input to this algorithm was the spike-density function on Canceled trials and latency-matched no-stop trials at two time-windows relative to SSRT: a 100ms window preceding SSRT and a 200ms window following SSRT. Variations in this temporal window did not result in a considerable change in the clustering algorithm output.

Modulation Identification. To determine modulation around the time of successful stopping we applied similar method to that previously used in this laboratory. Significant modulation was defined as the interval when the difference between SDF on Canceled and Latency-matched No-stop trials (referred to as difference function) exceeded 2 standard deviations above a baseline difference (during 100 ms pre-target period), measured during the period from -50 to

900ms relative to stop-signal and persisted for at least 100 ms, or for 50 ms if the difference exceeded 3 standard deviations above the 100ms pre-target baseline. Neurons often exhibited low firing rates as typical for executive control signals in medial frontal cortex. To minimize the influence of incidental fluctuations in firing rate due to low signal-to-noise ratio we convolved the SDF with a moving window of width 8ms. The modulation timing obtained from this method were validated by manual inspection. Latency-matching to canceled trials involved the inclusion of only those no-stop trials with RT > SSD + SSRT, because according to the race model, only on these trials the saccade would have been inhibited had the stop-signal been presented.
To determine modulation around the time of feedback tone (illustrated in **Figs 2b, 3b, and 4b**) we applied a similar method but contrasted the SDF on Canceled trials against the minimum value within a window spanning 500 ms before to 900 ms after the feedback tone. With a primary interest in modulation during the period of operant control on behavior (i.e., prior to feedback tone), modulations that start after 300 ms following the tone are not included.

Differentiating Narrow- vs. Broad-spiking neurons. Spike widths across our sample of neurons exhibited a bimodal distribution previously described [12]. Based on this distribution, we classified our neurons into narrow-spike or broad-spike width. Narrow spike-width neurons had peak-to-trough duration less than 250 µs and broad spike-width neurons had peak-to-trough duration greater than or equal to 250 µs.

Model-fitting approach. We fit neural activity (spiking activity or ERP amplitude) to models derived from each of the behavioral / task measures. These models are described in detail in **Supplementary Figure 2**. In brief, we considered models based on response conflict, associated error rate, SSD time and feedback tone time, and their associated hazard rates. These behavioral and task measures are often correlated, however, random variations between them allowed for their differentiation. Three SSD bins were considered, corresponding to early-, mid-, and late-SSDs. SSDs greater than ~350ms were not included because the number of successful canceled trials for those SSDs was too few for any sensible analysis.

The value of the behavioral / task measure associated with each model was calculated on a trial-by-trial basis and then averaged within each SSD bin for averaging. Note that whereas all models were considered for analysis of activity following the stop-signal (including facilitation in discharge rate following SSRT, and the N2, and P3 components), only SSD hazard rate and time models related to SSD were considered for the ramping activity prior to SSRT, and

feedback tone hazard rate and time models related to the feedback tone were considered for the ramping activity prior to the tone.

The spiking activity of neurons was measured for all trials from convolved spike data, standardized to the z-scale, and averaged within each SSD bin.

For response facilitation around the time of successful stopping, the average activity on latency-matched no-stop trials was subtracted from that on each Canceled trial (i.e., difference function was obtained) to eliminate the activity related to other processes prior to stop-signal appearance. The results presented in the Main Text (**Fig 2, Fig 4**) are based on this difference value. However, the conclusions of this study did not depend on whether the activity was sampled based on the difference function or only the activity on Canceled trials.

For the analysis related to the interval just preceding SSRT, activity was measured from Canceled trials and not the difference function because the processes during that period are indistinguishable from that on no-stop trials. For the analysis related to the interval just preceding the feedback tone, activity was measured from Canceled trials because although on both canceled and no-stop trials positive reinforcement was cued, the timing of the feedback on Canceled trials exhibited variability (**Supplementary Fig 2**).

A set of mixed-effects models were constructed and compared using Bayesian Information Criteria (BIC). Neural activity was modeled against each of the testing behavioral / task measures. The results reported here are based on the basic version for which, each model contains a main effect term corresponding to a behavioral / task parameter. The mixed-effects model allowed for modeling random intercepts grouped by neuron (for spiking activity) or session (for ERP analysis). All competing models had the same number of terms (i.e., the same degrees of freedom) and were z-transformed normalized to allow effective comparison between them. This allowed for differences in Bayesian Information Criteria to be an effective way to identify the best model. The model with the smallest BIC was identified as the best model, and the performance of the other models relative to the best are reported using ΔBIC. As recommended [72, 73], ΔBIC ($BIC_{best} – BIC_{competing}$) < 2 suggests a weak support against the competing model, 2 < ΔBIC < 6 suggests strong support against the competing model, and ΔBIC > 6 can completely rule out the competing model. More complex versions of these models resulted in similar conclusions.

For the analysis of ERPs, the same approach was taken except that the amplitude was measured by the mean normalized voltage (z-transformed) for each SSD in a +/-50ms window around a session-specific estimate of ERP peak. Latency-matched ERP polarization on no-stop trials were subtracted from Canceled trials. Similar results were obtained when a narrower

window (+/-25ms) around the peak or amplitude at the peak (+/-0 ms) were considered. Mixed-effects models were constructed in the same ways as above, grouped by session. This grouping accounts for the fact that ERP measures can have different overall amplitudes and variability on a session-by-session basis.

Mixed-effects models were performed using MATLAB's Statistical Toolbox.

Behavioral measurements. Eye position data was collected at 1 kHz using an EyeLink 1000 infrared eye-tracking system (SR Research, Kanata, Ontario, Canada). This was streamed to a single data acquisition system (MAP, Plexon, Dallas, TX) and amalgamated with other behavioral and neurophysiological data.

Cortical mapping and electrode placement. Chambers implanted over the medial frontal cortex were mapped using tungsten microelectrodes (2-4 MΩ, FHC, Bowdoin, ME) to apply 200ms trains of biphasic micro-stimulation (333 Hz, 200 µs pulse width). The SEF was identified as the area from which saccades could be elicited using < 50 µA of current [74-76]. In both monkeys, the SEF chamber was placed over the left hemisphere.

The location of the SEF makes it readily accessible for electrode array recordings of neurons across all cortical layers. A total of five penetrations were made into the cortex; two in monkey Eu, and three in monkey X. Three of these penetrations were perpendicular to the cortex. In monkey Eu, the perpendicular penetrations sampled activity at site P1, located 5mm lateral to the midline and 31mm anterior to the interaural line. In monkey X, the perpendicular penetrations sampled activity at site P2 and P3, located 5mm lateral to the midline and 29 and 30mm anterior to the interaural line, respectively. However, during the mapping of the bank of the cortical medial wall, we noted both monkeys had chambers place ~1mm to the right respective to the midline of the brain. This was confirmed through co-registered CT/MRI data. Subsequently, the stereotaxic estimate placed the electrodes at 4mm lateral to the cortical midline opposed to the skull-based stereotaxic midline.

Data acquisition and neural sampling. Spiking activity and local field potentials were recorded from five sites within the SEF using a 24-channel Plexon U-probe (Dallas, TX) with 150 µm interelectrode spacing allowing sampling from all layers. Penetrations to three of these sites were perpendicular to the cortex. The U-probes were 100 mm in length with 30 mm reinforced tubing, 210 µm probe diameter, 30° tip angle, and had 500 µm between the tip and first contact. Contacts were referenced to the probe shaft and grounded to the headpost. We used custom

built guide tubes consisting of 26-gauge polyether ether ketone (PEEK) tubing (Plastics One, Roanoke, VA) cut to length and glued into 19-gauge stainless steel hypodermic tubing (Small Parts Inc., Logansport, IN). This tubing had been cut to length, deburred, and polished so that they effectively support the U-probes as they penetrated dura and entered cortex. The stainless-steel guide tube provided mechanical support, while the PEEK tubing electrically insulated the shaft of the U-probe, and provided an inert, low-friction interface that aided in loading and penetration.

Microdrive adapters were fit to recording chambers with < 400 µm of tolerance and locked in place at a single radial orientation (Crist Instruments, Hagerstown, MD). After setting up hydraulic microdrives (FHC, Bowdoin, ME) on these adapters, pivot points were locked in place 9 by means of a custom mechanical clamp. Neither guide tubes nor U-probes were removed from the microdrives once recording commenced within a single monkey. These methods ensured that we were able to sample neural activity from precisely the same location relative to the chamber on repeated sessions.

All data were streamed to a single data acquisition system (MAP, Plexon, Dallas, TX). Time stamps of trial events were recorded at 500 Hz. Eye position data were streamed to the Plexon computer at 1 kHz using an EyeLink 1000 infrared eye-tracking system (SR Research, Kanata, Ontario, Canada).

Electrophysiology data were processed with unity-gain high-input impedance head stages (HST/32o25-36P-TR, Plexon). Spiking data were bandpass filtered between 100 Hz and 8 kHz and amplified 1000 times with a Plexon preamplifier, filtered in software with a 250 Hz high-pass filter and amplified an additional 32,000 times. Waveforms were digitized from -200 to 1200 µs relative threshold crossings at 40 kHz. Thresholds were typically set at 3.5 standard deviations from the mean. Single units were sorted online using a software window discriminator and refined offline using principal components analysis implemented in Plexon offline sorter.

Cortical depth and Layer assignment. The retrospective depth of the electrode array relative to grey matter was assessed through the alignment of several physiological measures. Firstly, the pulse artifact was observed on a superficial channel which indicated where the electrode was in contact with either the dura mater or epidural saline in the recording chamber; these pulsated visibly in synchronization with the heartbeat. Secondly, a marked increase of power in the gamma frequency range (40-80Hz) was observed at several electrode contacts, across all sessions. Previous literature has demonstrated elevated gamma power in superficial and middle layers relative to deeper layers [77-79]. Thirdly, an automated depth alignment procedure was

employed which maximized the similarity of CSD profiles evoked by passive visual stimulation between sessions [18].

Further support for the laminar assignments was provided by an analysis of the depths of SEF layers measured in histological sections visualized with Nissl, neuronal nuclear antigen (NeuN), Gallyas myelin, acetylcholinesterase (AChE), non-phosphorylated neurofilament H (SMI-32), and the calcium-binding proteins parvalbumin (PV), calbindin (CB), and calretinin (CR). Additional information about laminar structure was assessed through the pattern of cross-frequency phase-amplitude coupling across SEF layers. Owing to variability in the depth estimates and the indistinct nature of the L6 border with white matter, some units appeared beyond the average gray-matter estimate; these were assigned to the nearest cellular layer.

Analysis of EEG. EEG was recorded from the cranial surface with electrodes located over medial frontal cortex. Electrodes were referenced to linked ears using ear-clip electrodes (Electro-Cap International). The EEG from each electrode was amplified with a high-input impedance head stage (Plexon) and bandpass filtered between 0.7 and 170 Hz. Trials with blinks within 200ms before or after the analysis interval were removed.
First, we obtained the ERPs related to stopping, by subtracting that on Canceled from latency-matched no-stop trials. We found similar polarizations to that reported in human studies, and found similar and consistent time-course across sessions. The peak of N2 was selected at a time when the mean ERP aligned on stop-signal reached maximal negativity within a 150 to 250ms window from stop-signal. The peak of P3 was selected at a time when the mean ERP aligned on stop-signal reached maximal positivity within a 250 to 400ms window from stop-signal. The amplitude of these ERPs was estimated in different ways, all reaching similar conclusions: The amplitude at the peak, the average amplitude in a ±25, ±50, and ±75 ms widow around the peak. In the results reported here, ±50 ms is used because this window captures the most robust segment of these ERPs.

Relationship between N2/P3 and neural spiking

We use the same method used previously to establish the relationship between spiking activity and the ERN [12]. Single trial N2 and P3 amplitudes were normally distributed. Single trial spiking activity values, using only data from confirmed perpendicular penetrations, was the mean convolved spike data for that trial recorded from neurons in L2/3 and in L5/6 within ±50 ms surrounding N2 and P3 peaks. To account for intersession variations in ERN voltage and spike

counts, a fixed-effects adjustment was performed by centering each distribution on its mean and dividing by its most extreme value.

To examine the relationship between the EEG magnitude and the spiking activity, we conducted multiple linear regression on normalized data pooled across all sessions with a perpendicular penetration. Three factors were considered: (1) spiking activity in L2/3, (2) spiking activity in L5/6, and (3) SSD. Stop-signal must be included to ensure that any relationship between either ERP components and neural spiking is not simply because of the independent variations of both with SSD.

To measure the N2/P3 amplitudes robustly, we grouped rank-ordered single-trial ERP values into 20 successive bins. From trials in each bin, we calculated the mean ERN magnitude (dependent variable), the mean spike count (independent variable), and the fraction of error trials (dummy variable values for trials in each bin). Data from all sessions were combined for a pooled partial correlation. Each point in **Fig. 6** plots the paired values of the mean normalized EEG voltage and normalized activity for each of the 20 bins from every session.

Code availability

The analysis codes that were used for this study are available from the corresponding author upon request.

Data availability

The data that support the findings of this study are available from the corresponding author upon request.

Acknowledgments

The authors thank J. Elsey, M. Feurtado, M. Maddox, S. Motorny, J. Parker, M. Schall, C.R. Subraveti, and L. Toy for animal care and other technical assistance, and M. Matsumoto, P. Redgrave, E. Sigworth, A. Tomarken, and the reviewers for helpful discussions and comments on the manuscript. Imaging data was collected in the Vanderbilt Institute of Imaging Science. This work was supported by R01-MH55806 (JS), P30-EY08126 (JS), Canadian Institutes of Health Research (CIHR) Post-Doctoral Fellowship, and by Robin and Richard Patton through the E. Bronson Ingram Chair in Neuroscience (JS).

Author contributions

Experimental design, J.D.S. Data collection, J.D.S. Data analysis, A.S. and S.E. Interpretation and preparation of manuscript, A.S., S.E., and J.D.S.

Competing interests

The authors declare no competing interests.

REFERENCES

1. Verbruggen, F. & Logan, G.D. Models of response inhibition in the stop-signal and stop-change paradigms. *Neurosci Biobehav Rev* **33**, 647-661 (2009).
2. Emeric, E.E.*, et al.* Influence of history on saccade countermanding performance in humans and macaque monkeys. *Vision Res* **47**, 35-49 (2007).
3. Kolling, N.*, et al.* Value, search, persistence and model updating in anterior cingulate cortex. *Nat Neurosci* **19**, 1280-1285 (2016).
4. Shenhav, A., Cohen, J.D. & Botvinick, M.M. Dorsal anterior cingulate cortex and the value of control. *Nat Neurosci* **19**, 1286-1291 (2016).
5. Kok, A., Ramautar, J.R., De Ruiter, M.B., Band, G.P. & Ridderinkhof, K.R. ERP components associated with successful and unsuccessful stopping in a stop-signal task. *Psychophysiology* **41**, 9-20 (2004).
6. Cohen, M.X. A neural microcircuit for cognitive conflict detection and signaling. *Trends Neurosci* **37**, 480-490 (2014).
7. Stuphorn, V., Brown, J.W. & Schall, J.D. Role of supplementary eye field in saccade initiation: executive, not direct, control. *J Neurophysiol* **103**, 801-816 (2010).
8. Reinhart, R.M.*, et al.* Homologous mechanisms of visuospatial working memory maintenance in macaque and human: properties and sources. *J Neurosci* **32**, 7711-7722 (2012).
9. Bastos, A.M., Loonis, R., Kornblith, S., Lundqvist, M. & Miller, E.K. Laminar recordings in frontal cortex suggest distinct layers for maintenance and control of working memory. *Proc Natl Acad Sci U S A* **115**, 1117-1122 (2018).
10. Kawaguchi, N.*, et al.* Surprise signals in the supplementary eye field: rectified prediction errors drive exploration-exploitation transitions. *J Neurophysiol* **113**, 1001-1014 (2015).
11. Wang, J., Narain, D., Hosseini, E.A. & Jazayeri, M. Flexible timing by temporal scaling of cortical responses. *Nat Neurosci* **21**, 102-110 (2018).
12. Sajad, A., Godlove, D.C. & Schall, J.D. Cortical microcircuitry of performance monitoring. *Nat Neurosci* **22**, 265-274 (2019).
13. Amiez, C. & Petrides, M. Anatomical organization of the eye fields in the human and non-human primate frontal cortex. *Prog Neurobiol* **89**, 220-230 (2009).
14. Stuphorn, V. & Schall, J.D. Executive control of countermanding saccades by the supplementary eye field. *Nat Neurosci* **9**, 925-931 (2006).
15. Pouget, P.*, et al.* Neural basis of adaptive response time adjustment during saccade countermanding. *J Neurosci* **31**, 12604-12612 (2011).
16. Bastos, A.M.*, et al.* Canonical microcircuits for predictive coding. *Neuron* **76**, 695-711 (2012).
17. Shipp, S. The importance of being agranular: a comparative account of visual and motor cortex. *Philos Trans R Soc Lond B Biol Sci* **360**, 797-814 (2005).
18. Godlove, D.C., Maier, A., Woodman, G.F. & Schall, J.D. Microcircuitry of agranular frontal cortex: testing the generality of the canonical cortical microcircuit. *J Neurosci* **34**, 5355-5369 (2014).
19. Beul, S.F. & Hilgetag, C.C. Towards a "canonical" agranular cortical microcircuit. *Front Neuroanat* **8**, 165 (2014).
20. Ninomiya, T., Dougherty, K., Godlove, D.C., Schall, J.D. & Maier, A. Microcircuitry of agranular frontal cortex: contrasting laminar connectivity between occipital and frontal areas. *J Neurophysiol* **113**, 3242-3255 (2015).
21. Hanes, D.P. & Schall, J.D. Countermanding saccades in macaque. *Vis Neurosci* **12**, 929-937 (1995).
22. Verbruggen, F.*, et al.* A consensus guide to capturing the ability to inhibit actions and impulsive behaviors in the stop-signal task. *Elife* **8** (2019).
23. Logan, G.D. & Cowan, W.B. On the Ability to Inhibit Thought and Action - a Theory of an Act of Control. *Psychological Review* **91**, 295-327 (1984).
24. Hanes, D.P., Patterson, W.F., 2nd & Schall, J.D. Role of frontal eye fields in countermanding saccades: visual, movement, and fixation activity. *J Neurophysiol* **79**, 817-834 (1998).
25. Lowe, K.A. & Schall, J.D. Functional Categories of Visuomotor Neurons in Macaque Frontal Eye Field. *eNeuro* **5** (2018).
26. Boucher, L., Palmeri, T.J., Logan, G.D. & Schall, J.D. Inhibitory control in mind and brain: an interactive race model of countermanding saccades. *Psychol Rev* **114**, 376-397 (2007).

27. Logan, G.D., Yamaguchi, M., Schall, J.D. & Palmeri, T.J. Inhibitory control in mind and brain 2.0: blocked-input models of saccadic countermanding. *Psychol Rev* **122**, 115-147 (2015).
28. Botvinick, M.M., Braver, T.S., Barch, D.M., Carter, C.S. & Cohen, J.D. Conflict monitoring and cognitive control. *Psychol Rev* **108**, 624-652 (2001).
29. Brown, J.W. & Braver, T.S. Learned predictions of error likelihood in the anterior cingulate cortex. *Science* **307**, 1118-1121 (2005).
30. Nelson, M.J., Boucher, L., Logan, G.D., Palmeri, T.J. & Schall, J.D. Nonindependent and nonstationary response times in stopping and stepping saccade tasks. *Atten Percept Psychophys* **72**, 1913-1929 (2010).
31. Kim, J., Ghim, J.W., Lee, J.H. & Jung, M.W. Neural correlates of interval timing in rodent prefrontal cortex. *J Neurosci* **33**, 13834-13847 (2013).
32. Janssen, P. & Shadlen, M.N. A representation of the hazard rate of elapsed time in macaque area LIP. *Nat Neurosci* **8**, 234-241 (2005).
33. Gibbon, J. Scalar expectancy theory and Weber's law in animal timing. *Psychological review* **84**, 279 (1977).
34. Ohmae, S., Lu, X., Takahashi, T., Uchida, Y. & Kitazawa, S. Neuronal activity related to anticipated and elapsed time in macaque supplementary eye field. *Exp Brain Res* **184**, 593-598 (2008).
35. Zhang, K., Chen, C.D. & Monosov, I.E. Novelty, Salience, and Surprise Timing Are Signaled by Neurons in the Basal Forebrain. *Curr Biol* **29**, 134-142 e133 (2019).
36. Stuphorn, V., Taylor, T.L. & Schall, J.D. Performance monitoring by the supplementary eye field. *Nature* **408**, 857-860 (2000).
37. Schall, J.D. & Boucher, L. Executive control of gaze by the frontal lobes. *Cogn Affect Behav Neurosci* **7**, 396-412 (2007).
38. Errington, S.P. & Schall, J.D. Express saccades during a countermanding task. *J Neurophysiol* **124**, 484-496 (2020).
39. Tallot, L. & Doyere, V. Neural encoding of time in the animal brain. *Neurosci Biobehav Rev* **115**, 146-163 (2020).
40. Ogasawara, T., Nejime, M., Takada, M. & Matsumoto, M. Primate Nigrostriatal Dopamine System Regulates Saccadic Response Inhibition. *Neuron* **100**, 1513-1526 e1514 (2018).
41. Pare, M. & Hanes, D.P. Controlled movement processing: superior colliculus activity associated with countermanded saccades. *J Neurosci* **23**, 6480-6489 (2003).
42. Williams, S.M. & Goldman-Rakic, P.S. Widespread origin of the primate mesofrontal dopamine system. *Cereb Cortex* **8**, 321-345 (1998).
43. Huerta, M.F. & Kaas, J.H. Supplementary eye field as defined by intracortical microstimulation: connections in macaques. *J Comp Neurol* **293**, 299-330 (1990).
44. Shook, B.L., Schlag-Rey, M. & Schlag, J. Primate supplementary eye field: I. Comparative aspects of mesencephalic and pontine connections. *J Comp Neurol* **301**, 618-642 (1990).
45. Parthasarathy, H.B., Schall, J.D. & Graybiel, A.M. Distributed but convergent ordering of corticostriatal projections: analysis of the frontal eye field and the supplementary eye field in the macaque monkey. *J Neurosci* **12**, 4468-4488 (1992).
46. Thierry, A.M., Deniau, J.M., Herve, D. & Chevalier, G. Electrophysiological evidence for non-dopaminergic mesocortical and mesolimbic neurons in the rat. *Brain Res* **201**, 210-214 (1980).
47. Coull, J. & Nobre, A. Dissociating explicit timing from temporal expectation with fMRI. *Curr Opin Neurobiol* **18**, 137-144 (2008).
48. Herrera, B., Sajad, A., Woodman, G.F., Schall, J.D. & Riera, J.J. A Minimal Biophysical Model of Neocortical Pyramidal Cells: Implications for Frontal Cortex Microcircuitry and Field Potential Generation. *J Neurosci* **40**, 8513-8529 (2020).
49. Fiorillo, C.D., Newsome, W.T. & Schultz, W. The temporal precision of reward prediction in dopamine neurons. *Nat Neurosci* **11**, 966-973 (2008).
50. Vijayraghavan, S., Major, A.J. & Everling, S. Dopamine D1 and D2 Receptors Make Dissociable Contributions to Dorsolateral Prefrontal Cortical Regulation of Rule-Guided Oculomotor Behavior. *Cell Rep* **16**, 805-816 (2016).
51. Griggs, W.S.*, et al.* Flexible and Stable Value Coding Areas in Caudate Head and Tail Receive Anatomically Distinct Cortical and Subcortical Inputs. *Front Neuroanat* **11**, 106 (2017).
52. Mann, E.O., Kohl, M.M. & Paulsen, O. Distinct roles of GABA(A) and GABA(B) receptors in balancing and terminating persistent cortical activity. *J Neurosci* **29**, 7513-7518 (2009).

53. Ferguson, B.R. & Gao, W.J. PV Interneurons: Critical Regulators of E/I Balance for Prefrontal Cortex-Dependent Behavior and Psychiatric Disorders. *Front Neural Circuits* **12**, 37 (2018).
54. Medalla, M. & Barbas, H. Synapses with inhibitory neurons differentiate anterior cingulate from dorsolateral prefrontal pathways associated with cognitive control. *Neuron* **61**, 609-620 (2009).
55. Egger, S.W., Le, N.M. & Jazayeri, M. A neural circuit model for human sensorimotor timing. *Nat Commun* **11**, 3933 (2020).
56. Buhusi, C.V. & Meck, W.H. What makes us tick? Functional and neural mechanisms of interval timing. *Nat Rev Neurosci* **6**, 755-765 (2005).
57. Emmons, E.*, et al.* Temporal learning among prefrontal and striatal ensembles. *Cerebral Cortex Communications* **1**, tgaa058 (2020).
58. Sommer, M.A. & Wurtz, R.H. A pathway in primate brain for internal monitoring of movements. *Science* **296**, 1480-1482 (2002).
59. Xu, K.Z.*, et al.* Neural Basis of Cognitive Control over Movement Inhibition: Human fMRI and Primate Electrophysiology Evidence. *Neuron* **96**, 1447-1458 e1446 (2017).
60. Gidon, A. & Segev, I. Principles governing the operation of synaptic inhibition in dendrites. *Neuron* **75**, 330-341 (2012).
61. Huster, R.J., Messel, M.S., Thunberg, C. & Raud, L. The P300 as marker of inhibitory control - Fact or fiction? *Cortex* **132**, 334-348 (2020).
62. Smith, J.L., Smith, E.A., Provost, A.L. & Heathcote, A. Sequence effects support the conflict theory of N2 and P3 in the Go/NoGo task. *Int J Psychophysiol* **75**, 217-226 (2010).
63. Lo, C.C., Boucher, L., Pare, M., Schall, J.D. & Wang, X.J. Proactive inhibitory control and attractor dynamics in countermanding action: a spiking neural circuit model. *J Neurosci* **29**, 9059-9071 (2009).
64. Thakkar, K.N., Schall, J.D., Boucher, L., Logan, G.D. & Park, S. Response inhibition and response monitoring in a saccadic countermanding task in schizophrenia. *Biol Psychiatry* **69**, 55-62 (2011).
65. Hubel, D.H. & Wiesel, T.N. Receptive fields and functional architecture of monkey striate cortex. *J Physiol* **195**, 215-243 (1968).
66. Godlove, D.C., Garr, A.K., Woodman, G.F. & Schall, J.D. Measurement of the extraocular spike potential during saccade countermanding. *J Neurophysiol* **106**, 104-114 (2011).
67. Kawagoe, R., Takikawa, Y. & Hikosaka, O. Expectation of reward modulates cognitive signals in the basal ganglia. *Nat Neurosci* **1**, 411-416 (1998).
68. Camalier, C.R.*, et al.* Dynamics of saccade target selection: race model analysis of double step and search step saccade production in human and macaque. *Vision Res* **47**, 2187-2211 (2007).
69. Matzke, D., Dolan, C.V., Logan, G.D., Brown, S.D. & Wagenmakers, E.J. Bayesian parametric estimation of stop-signal reaction time distributions. *J Exp Psychol Gen* **142**, 1047-1073 (2013).
70. Matzke, D.*, et al.* Release the BEESTS: Bayesian Estimation of Ex-Gaussian STop-Signal reaction time distributions. *Front Psychol* **4**, 918 (2013).
71. Matzke, D., Love, J. & Heathcote, A. A Bayesian approach for estimating the probability of trigger failures in the stop-signal paradigm. *Behav Res Methods* **49**, 267-281 (2017).
72. Raftery, A.E. Bayesian model selection in social research. *Sociological methodology*, 111-163 (1995).
73. Kass, R.E. & Raftery, A.E. Bayes factors. *Journal of the american statistical association* **90**, 773-795 (1995).
74. Schall, J.D. Neuronal activity related to visually guided saccades in the frontal eye fields of rhesus monkeys: comparison with supplementary eye fields. *J Neurophysiol* **66**, 559-579 (1991).
75. Martinez-Trujillo, J.C., Medendorp, W.P., Wang, H. & Crawford, J.D. Frames of reference for eye-head gaze commands in primate supplementary eye fields. *Neuron* **44**, 1057-1066 (2004).
76. Thompson, K.G., Hanes, D.P., Bichot, N.P. & Schall, J.D. Perceptual and motor processing stages identified in the activity of macaque frontal eye field neurons during visual search. *J Neurophysiol* **76**, 4040-4055 (1996).
77. Maier, A., Adams, G.K., Aura, C. & Leopold, D.A. Distinct superficial and deep laminar domains of activity in the visual cortex during rest and stimulation. *Front Syst Neurosci* **4** (2010).
78. Xing, D., Yeh, C.I., Burns, S. & Shapley, R.M. Laminar analysis of visually evoked activity in the primary visual cortex. *Proc Natl Acad Sci U S A* **109**, 13871-13876 (2012).

79. Smith, M.A. & Sommer, M.A. Spatial and temporal scales of neuronal correlation in visual area V4. *J Neurosci* **33**, 5422-5432 (2013).

FIGURES

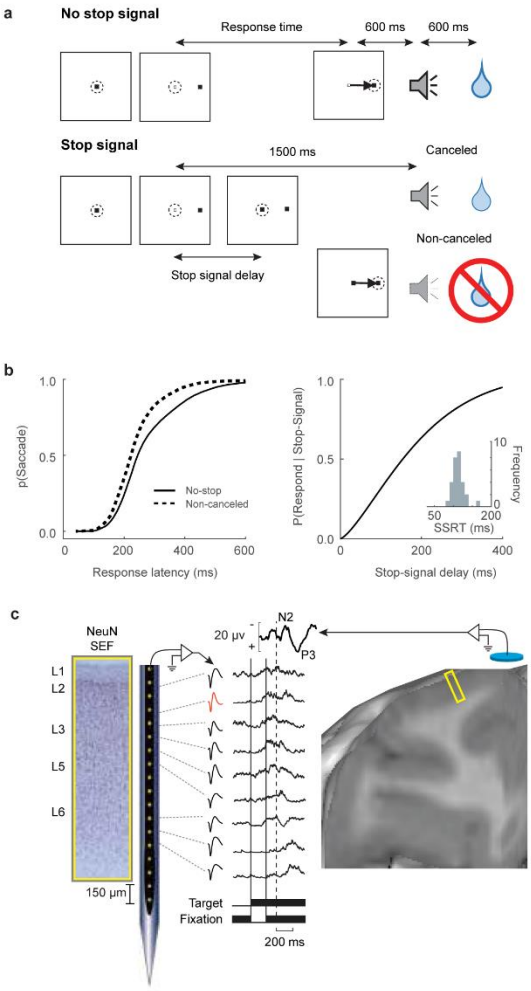

Fig. 1 | Experimental approach. a, Saccade countermanding task. Monkeys initiated trials by fixating a central point. After a variable time, the center of the fixation point was extinguished. A peripheral target was presented simultaneously at one of two possible locations. On no stop-signal trials monkeys were required to shift gaze to the target, whereupon after 600 ± 0 ms a high-pitch auditory feedback tone was delivered, and 600 ± 0 ms later fluid reward was provided. On stop-signal trials (~40% of trials) after the target appeared, the center of the fixation point was re-illuminated after a variable stop-signal delay, which instructed the monkey to cancel the saccade in which case the same high-pitch tone was presented after a 1,500 ± 0 ms hold time followed after 600 ± 0 ms by fluid reward. Stop-signal delay was adjusted such that monkeys successfully canceled the saccade in ~50% of trials. In the remaining trials, monkeys made non-canceled errors, which were followed after 600 ± 0 ms by a low-pitch tone, and no reward was delivered. Monkeys could not initiate trials earlier after errors. **b,** Cumulative distributions of all RT for both monkeys on trials with no stop-signal (solid) and non-canceled

errors (dashed). **c,** Probability of non-canceled errors as a function of stop-signal delay. Each symbol plots value from each session. Symbol size is proportional to number of trials measured. **d,** Distribution of SSRT across all sessions for both monkeys. **e,** RT on no-stop trials following no-stop (white), non-canceled (light blue), and canceled (dark blue) trials. **f,** Neural spiking was recorded across all layers of agranular SEF (NeuN stain) using Plexon U-probe. Neurons with both broad (black) and narrow (red) spikes were sampled (middle), and spike density was measured relative to presentation of task events like the visual target and the stop-signal (solid vertical lines) and the inferred SSRT (dashed vertical line). Simultaneously, EEG was recorded from the cranial surface with an electrode (blue disk) positioned over the medial frontal cortex (10-20 location Fz). Yellow rectangle portrays cortical area sampled in a T1 MR image.

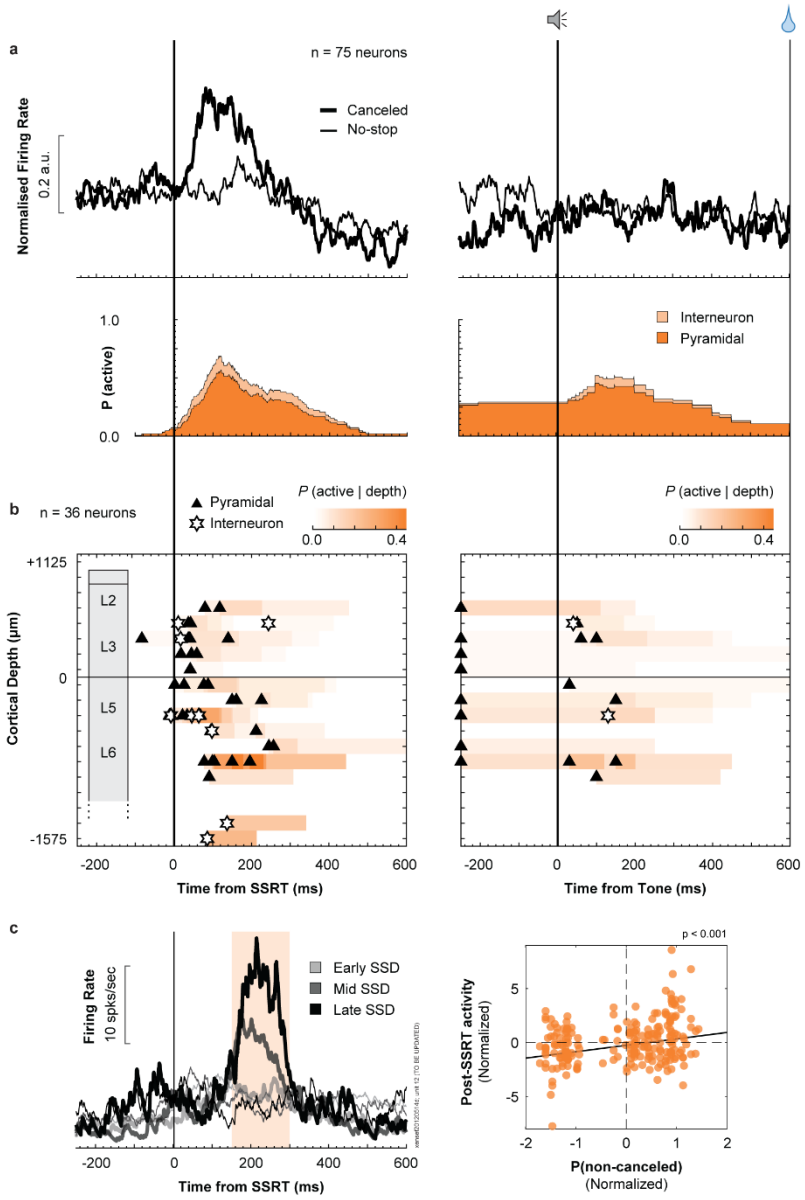

Fig. 2 | Time-depth organization of Conflict neuron spiking in SEF. a, Normalized population response of neurons with transient facilitation in discharge rate on successfully Canceled (thick) relative to latency-matched No-stop (thin) trials for early SSD (top). Recruitment of this signal through time relative to SSRT (left) and auditory feedback tone (right), with dark and light shades representing the recruitment of broad-spiking (spike width ≥ 250 µs) and narrow-spiking (< 250 µs) neurons (bottom). Recruitment on SSRT-aligned activity (left panel) is defined as the difference between Canceled and No-stop trials. Recruitment on tone-aligned activity (right panel) is defined as the activity on Canceled trials relative to the baseline. Modulations starting 300ms after the tone are not included. **b,** Time-depth plot showing latency and proportion of recruited neurons through time at each depth from perpendicular penetrations. Symbols mark beginning of modulation for broad-spiking neurons (black triangles) and narrow-

spiking neurons (white stars). Color map indicates the percentage of neurons producing this signal through time at each depth. Dashed horizontal line marks L3-L5 boundary. The lower boundary of L6 is not discrete. **c (left),** Comparison of response of a representative neuron on successfully canceled (thick) relative to latency-matched no-stop (thin) trials for low (lighter) and higher (darker) P(non-cancel). Shaded area represents significant difference in discharge rate between the two conditions. **c (right)** Relationship between spike rate, sampled from the period with significant modulation for each neuron and the corresponding P(non-cancel). Along the ordinate scale is plotted the firing rate, adjusted for neuron-specific variations. Along the abscissa scale is plotted the normalized P(non-cancel) (z-scale). In all, 225 points are plotted. Variation of firing rate was best predicted by P(non-cancel) (highlighted by the best-fit line; **Supplementary Table 2**).

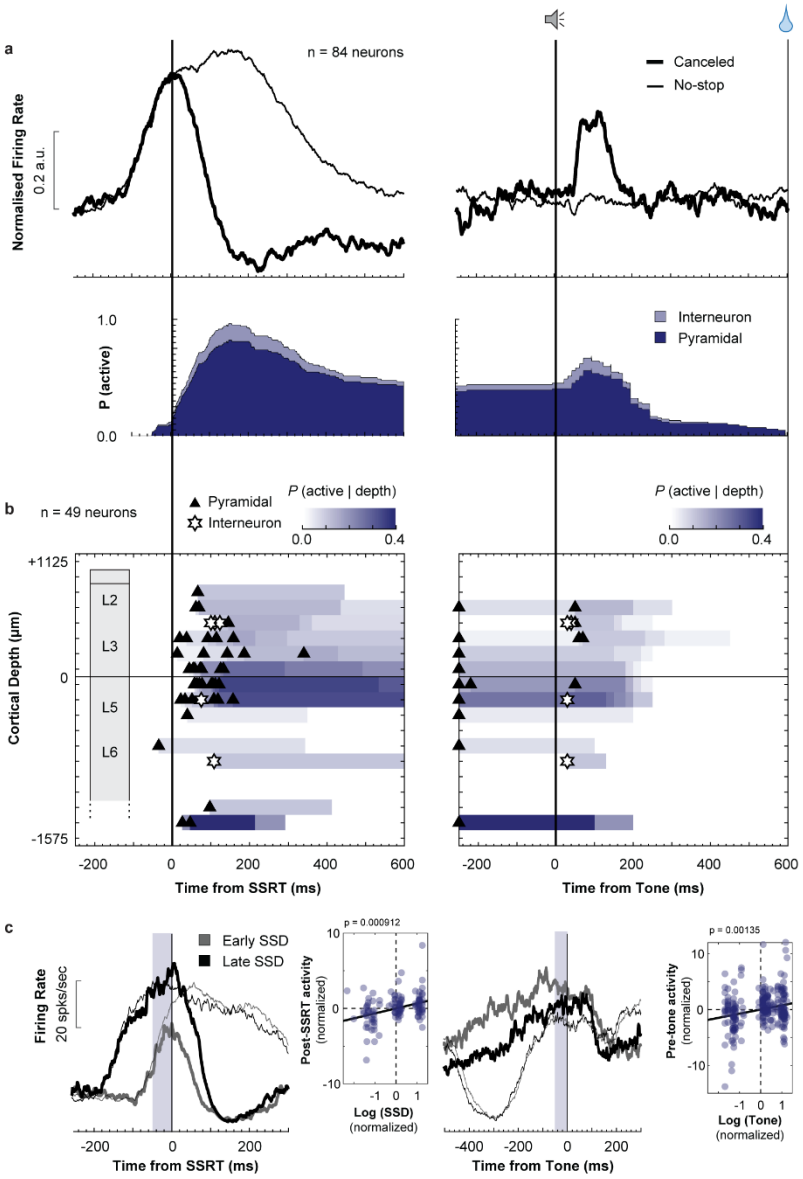

Fig. 3 | Time-depth organization of Event Timing neuron spiking in SEF. a, Normalized population response of neurons with suppression of discharge rate on successfully canceled (thick) relative to latency-matched no-stop (thin) trials for early SSD (bottom). Recruitment of signal through time relative to SSRT (left) and auditory feedback tone (right), with dark and light shades representing the recruitment of broad-spiking (spike width ≥ 250 µs) and narrow-spiking (< 250 µs) neurons (bottom). Recruitment on SSRT-aligned activity (left panel) is defined as the difference between Canceled and No-stop trials. Recruitment on tone-aligned activity (right panel) is defined as the activity on Canceled trials relative to the baseline. Modulations starting 300ms after the tone are not shown. **b,** Time-depth plot showing latency and proportion of recruited neurons through time at each depth from perpendicular penetrations. Symbols mark beginning of modulation for broad-spiking neurons (black triangles) and narrow-spiking neurons

(white stars). Color map indicates the percentage of neurons producing this signal through time at each depth. Dashed horizontal line marks L3-L5 boundary. The lower boundary of L6 is not discrete. **c, (left)** Response of a representative neurons on successfully canceled (thick) and latency-matched no-stop (thin) trials for early (lighter) and later (darker) SSD. Pre-SSRT ramping activity occurs irrespective of trial type. Shaded area represents the time epoch used for sampling neuron activity (50 ms window pre-SSRT). **c, (right)** Relationship between discharge rate in the sampling interval and stop-signal delay. Along the ordinate scale is plotted the normalized firing rate, adjusting for neuron-specific variations. Along the abscissa scale is plotted the normalized (z-transformed) stop-signal delay in logarithmic scale. In all, 252 points (84 neurons) are plotted. Each point plots the average spike-density and associated Log (SSD) in one of 3 bins corresponding to early-, mid-, or late-SSD, for each neuron. Variation of firing rate was best predicted by the time of the stop-signal (highlighted by best-fit line). **d, (left)** Response of the same representative neuron as **c** indicating pre-tone ramping activity on successfully canceled (thick) relative to latency-matched no-stop (thin) trials for early (lighter) and later (darker) SSD. Shaded area represents the time epoch used for sampling neuron activity (50 ms window pre-Tone). **d, (right)** Relationship between discharge rate in the sampling interval and the time of feedback relative to stop-signal. Along the ordinate scale is plotted the firing rate, adjusted for neuron-specific variations. Along the abscissa scale is plotted the normalized stop-signal delay in logarithmic scale (z-scale). In all, 144 points (38 neurons with pre-tone activity on Canceled trials) are plotted. Each point plots the average spike-density and associated log (feedback time) in one of 3 bins corresponding to early-, mid-, or late-SSD, for each neuron. Variation of firing rate was best predicted by the time of the feedback time (highlighted by best-fit line; **Supplementary Table 2**).

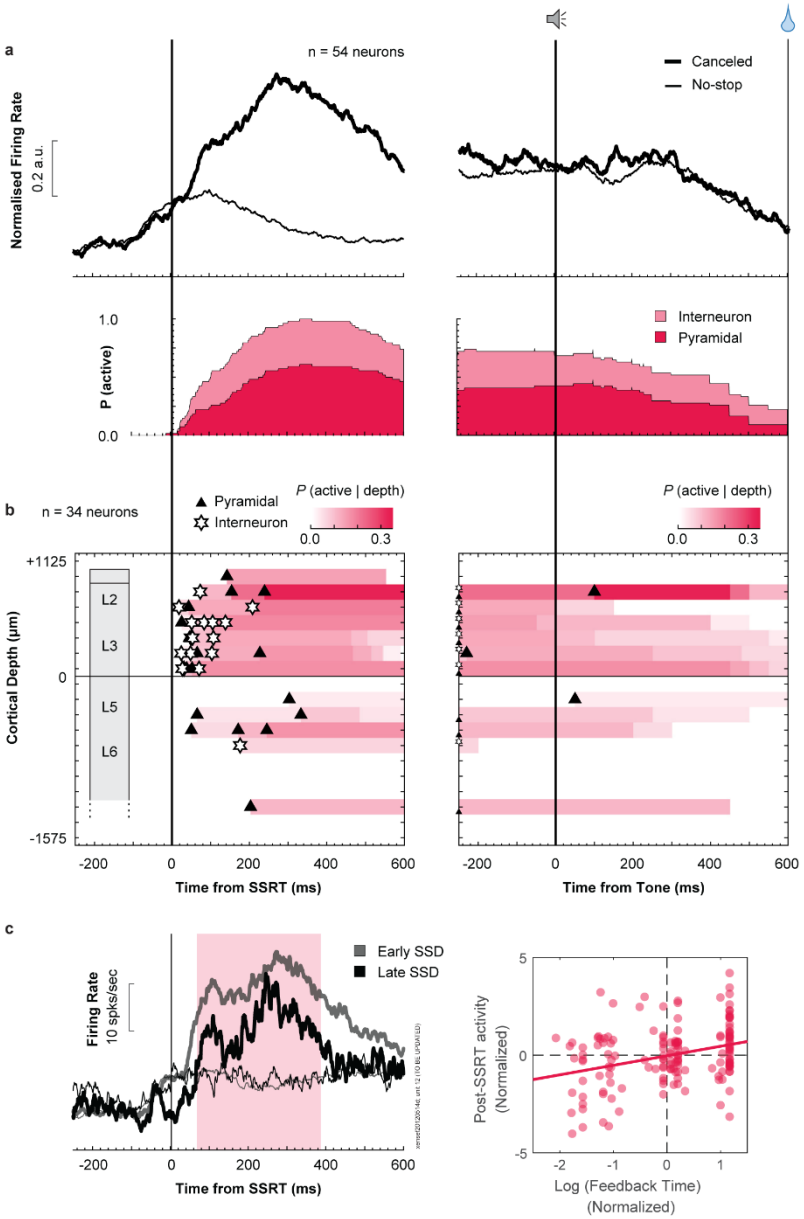

Fig. 4 | Time-depth organization of Goal Maintenance neuron spiking in SEF. a, Normalized population response of neurons with prolonged facilitation in discharge rate on successful canceled (thick) relative to latency-matched no-stop (thin) trials for early SSD. **b,** Recruitment of this signal through time relative to SSRT (left) and auditory feedback tone (right), with dark and light shades representing the recruitment of broad-spiking (spike width ≥ 250 µs) and narrow-spiking (< 250 µs) neurons. Recruitment on SSRT-aligned activity (left panel) is defined as the difference between Canceled and No-stop trials. Recruitment on tone-aligned activity (right panel) is defined as the activity on Canceled trials relative to the baseline. Modulations starting 300ms after the tone are not shown. **c,** Time-depth plot showing latency and proportion of recruited neurons through time at each depth from perpendicular penetrations. Symbols mark beginning of modulation for broad-spiking neurons (black triangles) and narrow-

spiking neurons (white stars). Color map indicates the percentage of neurons producing this signal through time at each depth. Dashed horizontal line marks L3-L5 boundary. The lower boundary of L6 is not discrete. **d (left),** Comparison of response of a representative neuron on successfully canceled (thick) relative to latency-matched no-stop (thin) trials for early (lighter) and later (darker) SSD. Shaded area represents significant difference in discharge rate between the two conditions. **d (right)** Relationship between discharge rate in the sampling interval and feedback tone time. Along the ordinate scale is plotted the firing rate, adjusted for neuron-specific variations. Along the abscissa scale is plotted the normalized feedback time in logarithmic scale (z-scale). In all, 162 points (54 neurons) are plotted. Each point plots the average spike-density and associated Log (feedback time) in one of 3 bins corresponding to early-, mid-, or late-SSD, for each neuron. Variation of firing rate was best predicted by the time of the feedback time (highlighted by best-fit line; **Supplementary Table 2**).

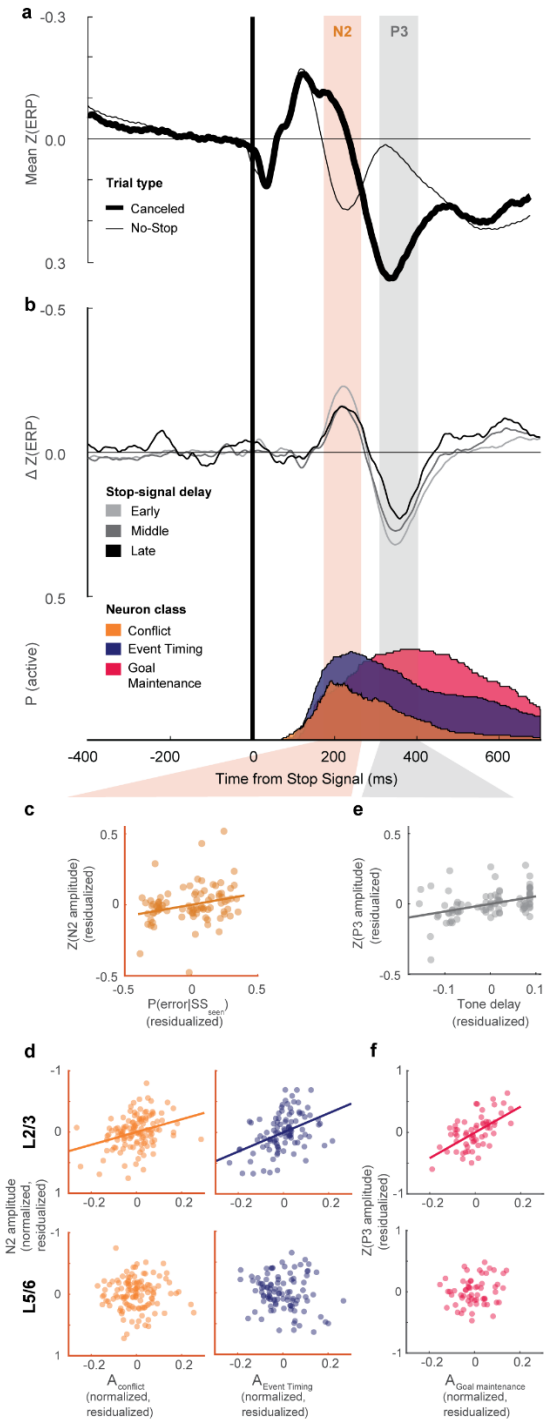

Fig. 5 | Event-related potentials for successful response inhibition. a, Grand average normalized EEG (z-transformed) on successful canceled (thick) relative to latency-matched no-stop (thin) trials for early SSD. **b,** the difference function highlights the N2 and P3 components, eliminating the effect of response stimulus-evoked ERP common to both canceled and no-stop trials. The shaded regions correspond to a ±50 ms sampling window around peak of N2 (orange) and P3 (gray) used for ERP amplitude calculation for **c**. **c,** Relationship between N2

amplitude and P (error | SSDseen). Along the ordinate scale, the normalized ERP amplitude is plotted, adjusting for session-specific variations. Along the abscissa scale the normalized P (error | SSDseen) is plotted (**Supplementary Fig 2c**). In all, 87 points (29 sessions) are plotted. Each point plots the average N2 and the associated P (error | SSDseen) in one of 3 bins corresponding to early-, mid-, or late-SSD, for each session. P (error | SSDseen) is the best parameter that described variations in N2 (highlighted by best-fit line). **d,** Relationship between P3 amplitude and the time of feedback relative to stop-signal. Along the ordinate scale is plotted the normalized ERP amplitude (z-scale), adjusted for session-specific variations in amplitude. Along the abscissa scale is plotted the normalized feedback time in logarithmic scale (z-scale). In all, 87 points (29 sessions) are plotted with each point plotting the average spike-density and associated Log (feedback time) in one of 3 bins corresponding to early-, mid-, or late-SSD, for each neuron. Variation of P3 amplitude was best predicted by the time of the feedback time (highlighted by best-fit line; **Supplementary Table 2**). **e,** Relationship between laminar neuronal discharge rate and N2. From sessions with perpendicular penetrations, relationship between ERP amplitude and spike rate for Conflict neurons (A_{Conflict}), Event-Timing neurons ($A_{\text{Event Timing}}$), recorded in L2/3 (top) and L5/6 (bottom). Partial regression plots are obtained by plotting on the ordinate scale, according to EEG convention, the residual from fixed-effects-adjusted ERP amplitude controlling for activity in the opposite layer and stop-signal delay. Along the abscissa scale is plotted the residual fixed-effects-adjusted neuronal discharge rate in the identified layer controlling for the activity in the opposite layer and stop-signal delay. Each point plots the average EEG voltage and associated firing rate in one of 20 bins with equal numbers of trials per session. Only sessions with neurons in both L2/3 and L5/6 are included. A total of 120 points (from 6 session) are plotted for Conflict Neurons (left), and 100 points (5 sessions) are plotted for Event-Timing neurons (right). The relationship between N2 and other neurons not reported in this study and Goal Maintenance neurons are shown in **Supplementary Fig 7a**. Variations in N2 amplitude was predicted by variation of firing rate of Conflict and Event-Timing neurons in L2/3 (highlighted by best-fit line) but not in L5/6. **f,** Relationship between laminar neuronal discharge rate and P3. From sessions with perpendicular penetrations, relationship between ERP amplitude and spike rate for Goal Maintenance neurons ($A_{\text{Goal Maintenance}}$), recorded in L2/3 (top) and L5/6 (bottom). Partial regression plots are obtained by plotting on the ordinate scale, according to EEG convention, the residual from fixed-effects-adjusted ERP amplitude controlling for activity in the opposite layer and stop-signal delay. Similar conventions to panel **e**. Only sessions with neurons in both L2/3 and L5/6 are included. A total of 60 points (from 3 sessions) are plotted for Goal Maintenance neurons. The relationship between P3 and other neuron types are shown in **Supplementary Fig 7c**. Variations in P3 amplitude was predicted by variation of firing rate of Goal Maintenance neurons in L2/3 (highlighted by best-fit line) but not in L5/6.

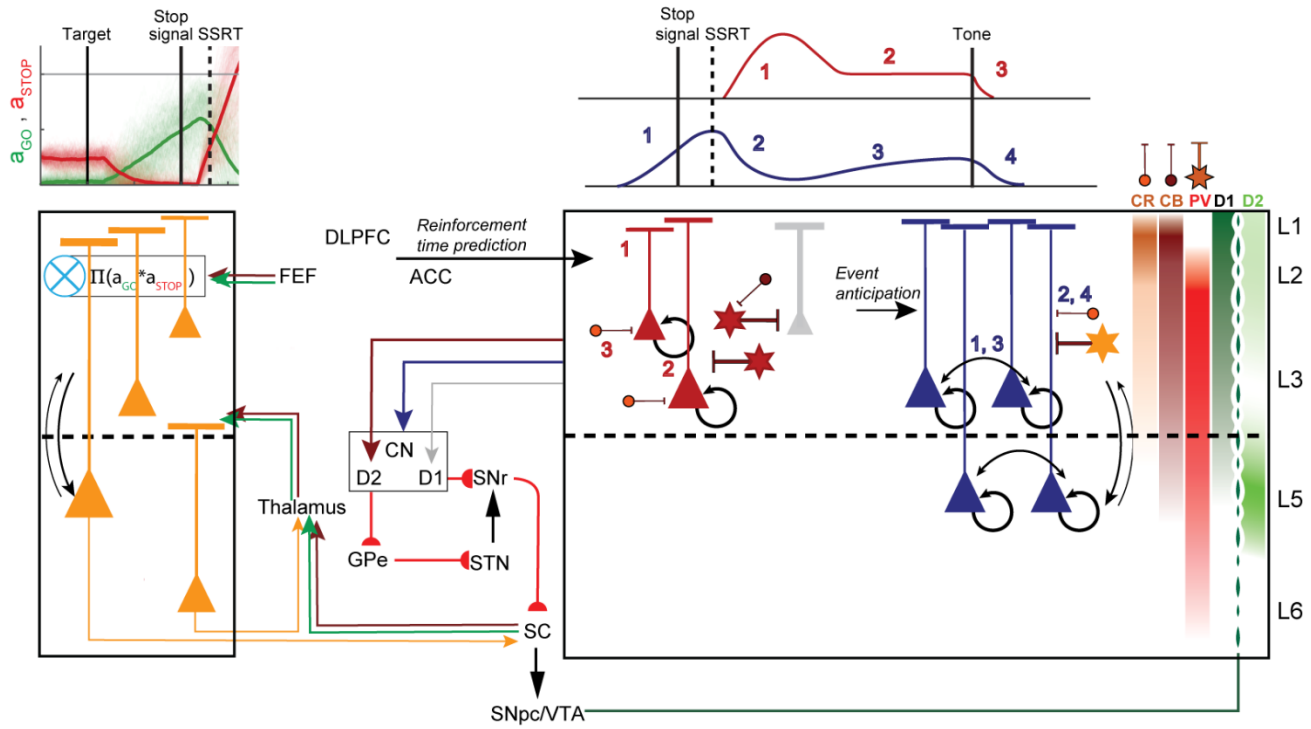

Fig 6 | Extrinsic and intrinsic circuitry for executive control. The laminar distribution observed for Conflict (orange), Goal Maintenance (dark red), and Event-timing (dark blue) are summarized with selected anatomical connections based on published studies. Sampled neurons were likely Pyramidal (triangles) and inhibitory PV neurons (stars). The laminar density of calretinin (CR, orange), calbindin (CB, brown), and parvalbumin (PV, red) neurons, as well as D1 and D2 receptors is indicated on the far right. **Left**, Conflict signal can arise in SEF through afferents from frontal eye field (FEF). SEF can receive coincident inputs from Fixation neurons (STOP) and Movement neurons (GO) in FEF, directly, or in SC, indirectly, via thalamus, terminating in L2/3. These inputs are integrated within the synapses of L2/3 and L5 Conflict neurons. Intracortical processing produces later activation of Conflict neurons in L6 which can relay this signal to the Thalamus. **Right**, Top: Schematic of the activity profile for Goal Maintenance and Event-timing neurons in distinct phases indicated by the number. We conjecture that Goal Maintenance neurons, mainly located in L2/3, suppress unwanted movement through push-pull basal ganglia circuitry with pyramidal neurons directly projecting to the indirect pathway (D2) and inhibitory neurons, inhibiting pyramidal neurons that can project to the direct (D1) pathway. The gray symbol indicates that these neurons are distinct from those reported in this study. Input from dorsolateral prefrontal cortex (DLPFC) and anterior cingulate cortex (ACC), terminating in L2/3 can inform SEF of the anticipated reward association based on the experienced stop-signal delay contingent on successful stopping. Dopamine (DA) neuron projections in L2/3 from the VTA can also relay this information (Green bulges on the right represented the en-passant endings of DA terminals). These inputs can result in the phasic response in Goal Maintenance neurons (phase 1, red). Following the phasic response, activity can remain elevated via recurrent connections and balance of excitation and inhibition (phase 2,

red). The auditory feedback tone, integrated with the task rule from DLPFC cues the termination of operant control on behavior, resulting in the inhibition of pyramidal and inter-neurons by CR and CB neurons. This results in the termination of the sustained activity (phase 3). Event Timing neurons can receive input from DLPFC and ACC terminating in L2/3 informing neurons in L2/3 and L5 about an upcoming event. Ramping results from recurrent connections (1, dark blue). SEF can receive information about stop-signal appearance and successful stopping from ventrolateral prefrontal cortex (VLPFC) and DLPFC and Conflict neurons within the microcircuitry. This information can suppress the ramping activity via inhibitory connections by direct inhibitory connections onto Event Timing neurons (phase 2, dark blue). This resets these neurons for the next phase of ramping (phase 3, dark blue) which is terminated by the appearance of the feedback tone (4). The activity of Event-timing neurons can project to the caudate nucleus to inform the fronto-striatal reinforcement learning loop about the experienced timing of the event. Further details in text.